

# The UVES Large Program for Testing Fundamental Physics: I Bounds on a change in $\alpha$ towards quasar HE 2217–2818 $\star$

P. Molaro<sup>1,7</sup>, M. Centurion<sup>1</sup>, J. B. Whitmore<sup>2</sup>, T. M. Evans<sup>2</sup>, M. T. Murphy<sup>2</sup>, I. I. Agafonova<sup>3</sup>, P. Bonifacio<sup>4</sup>, S. D’Odorico<sup>5</sup>, S. A. Levshakov<sup>3,12</sup>, S. Lopez<sup>6</sup>, C. J. A. P. Martins<sup>7</sup>, P. Petitjean<sup>8</sup>, H. Rahmani<sup>10</sup>, D. Reimers<sup>9</sup>, R. Srianand<sup>10</sup>, G. Vladilo<sup>1</sup>, M. Wendt<sup>11,9</sup>

<sup>1</sup> INAF-Osservatorio Astronomico di Trieste, Via G. B. Tiepolo 11, 34131 Trieste, Italy  
e-mail: molaro@oats.inaf.it

<sup>2</sup> Centre for Astrophysics and Supercomputing, Swinburne University of Technology, Hawthorn, VIC 3122, Australia

<sup>3</sup> Ioffe Physical-Technical Institute, Polytekhnicheskaya, Str. 26, 194021 Saint Petersburg, Russia

<sup>4</sup> GEPI, Observatoire de Paris, CNRS, Univ. Paris Diderot, Place Jules Janssen, 92190 Meudon, France

<sup>5</sup> ESO Karl, Schwarzschild-Str. 1 85741 Garching, Germany

<sup>6</sup> Departamento de Astronomia, Universidad de Chile, Casilla 36-D, Santiago, Chile

<sup>7</sup> Centro de Astrofísica, Universidade do Porto, Rua das Estrelas, 4150-762 Porto, Portugal

<sup>8</sup> Université Paris 6, Institut d’Astrophysique de Paris, CNRS UMR 7095, 98bis bd Arago, 75014 Paris, France

<sup>9</sup> Hamburger Sternwarte, Universität Hamburg, Gojenbergsweg 112, 21029 Hamburg, Germany

<sup>10</sup> Inter-University Centre for Astronomy and Astrophysics, Post Bag 4, Ganeshkhind, 411 007 Pune, India

<sup>11</sup> Institut für Physik und Astronomie, Universität Potsdam, 14476 Golm, Germany

<sup>12</sup> St. Petersburg Electrotechnical University ‘LETI’, Prof. Popov Str. 5, 197376 St. Petersburg, Russia

Received September 13, 2018; accepted September 13, 2018

## ABSTRACT

**Context.** Absorption-line systems detected in quasar spectra can be used to compare the value of the fine-structure constant,  $\alpha$ , measured today on Earth with its value in distant galaxies. In recent years, some evidence has emerged of small temporal and also spatial variations of  $\alpha$  on cosmological scales which may reach a fractional level of  $\approx 10$  ppm (parts per million).

**Aims.** To test these claims we are conducting a “Large Program” of observations with the Very Large Telescope’s Ultraviolet and Visual Echelle Spectrograph (UVES). We are obtaining high-resolution ( $R \approx 60000$ ) and high signal-to-noise ratio ( $S/N \approx 100$ ) UVES spectra calibrated specifically for this purpose. Here we analyse the first complete quasar spectrum from this Program, that of HE 2217–2818.

**Methods.** We apply the Many Multiplet method to measure  $\alpha$  in 5 absorption systems towards this quasar:  $z_{\text{abs}} = 0.7866, 0.9424, 1.5558, 1.6279$  and  $1.6919$ .

**Results.** The most precise result is obtained for the absorber at  $z_{\text{abs}} = 1.6919$  where 3 Fe II transitions and Al II  $\lambda 1670$  have high  $S/N$  and provide a wide range of sensitivities to  $\alpha$ . The absorption profile is complex, with several very narrow features, and requires 32 velocity components to be fitted to the data. We also conducted a range of tests to estimate the systematic error budget. Our final result for the relative variation in  $\alpha$  in this system is  $\Delta\alpha/\alpha = +1.3 \pm 2.4_{\text{stat}} \pm 1.0_{\text{sys}}$  ppm. This is one of the tightest current bounds on  $\alpha$ -variation from an individual absorber. A second, separate approach to the data-reduction, calibration and analysis of this system yielded a slightly different result of  $-3.8 \pm 2.1_{\text{stat}}$  ppm, possibly suggesting a larger systematic error component than our tests indicated. This approach used an additional 3 Fe II transitions, parts of which were masked due to contamination by telluric features. Restricting this analysis to the Fe II transitions only and using a modified absorption profile model, gave a result consistent with the first approach,  $\Delta\alpha/\alpha = +1.1 \pm 2.6_{\text{stat}}$  ppm. The other 4 absorbers have simpler absorption profiles, with fewer and broader features, and offer transitions with a smaller range of sensitivities to  $\alpha$ . Therefore, they provide looser bounds on  $\Delta\alpha/\alpha$  at the  $\geq 10$  ppm precision level.

**Conclusions.** The absorbers towards quasar HE 2217–2818 reveal no evidence for variation in  $\alpha$  at the 3-ppm precision level ( $1\text{-}\sigma$  confidence). If the recently-reported 10-ppm dipolar variation of  $\alpha$  across the sky were correct, the expectation at this sky position is  $(3.2\text{--}5.4) \pm 1.7$  ppm depending on dipole model used. Our constraint of  $\Delta\alpha/\alpha = +1.3 \pm 2.4_{\text{stat}} \pm 1.0_{\text{sys}}$  ppm is not inconsistent with this expectation.

**Key words.** Cosmology: observations – quasars: absorption lines – quasars: individual: quasar HE 2217–2818

## 1. Introduction

Metal lines of absorption systems due to intervening galaxies along the line of sight towards distant quasars provide insights into the atomic structure at the cosmic time and location of the

intervening object. All atomic transitions depend on the fine-structure constant, offering a way to probe possible variations of its value in space and time. The seminal papers of Savedoff (1956) and Bahcall et al. (1967) took advantage of the dependence of the relative separation of fine-structure doublet transitions on  $\alpha$  and used the alkali doublets observed in the first extragalactic sources to limit  $\Delta\alpha/\alpha$  at the level of a few percent. More recently, the many-multiplet (MM) method has been in-

Send offprint requests to: P. Molaro

$\star$  Based on observations taken at ESO Paranal Observatory. Program L 185.A-0745

roduced, which allows all observed transitions to be compared, gaining access to the typically much larger dependence of the ground state energy levels on  $\alpha$  (Dzuba et al. 1999). Overall, the MM method improves the sensitivity to the measurement of a variation of  $\alpha$  by more than an order of magnitude over the alkali-doublet method. Moreover, the individual dependence on  $\alpha$  of different atoms and transitions allows better control of instrumental and astrophysical systematic errors.

A first analysis using the many-multiplet method on quasar absorption spectra obtained at the Keck telescope revealed hints that in the early universe the fine structure constant was smaller than today by  $\sim 6$  parts-per-million (ppm; Webb et al. 1999; Murphy et al. 2001, 2003). However, the analysis of smaller data sets obtained from the Very Large Telescope (VLT) in Chile by other groups did not confirm the variation of  $\alpha$  (Quast et al. 2004; Chand et al. 2004; Levshakov et al. 2005, 2006), though in some cases these analysis and uncertainty estimates have been challenged (Murphy et al. 2007b, 2008) (but see Srianand et al. 2007). A recent analysis has been performed on a new sample built up by merging 141 measurements from Keck with 154 measurements from VLT (Webb et al. 2011; King et al. 2012). The merged sample indicates a spatial variation in  $\alpha$  across the sky at the  $4.1\sigma$  level with amplitude  $\sim 10$  ppm. Since the Keck telescope in Hawaii is at a latitude of  $20^\circ$  N, and the VLT in Chile is at latitude of  $25^\circ$  S, the two sub-samples survey relatively different hemispheres and the study of the merged sample provides a much more complete sky coverage. Remarkably, the two sets of measurements are consistent along the region of the sky covered by the two telescopes. So far, this spatial variation is formally consistent with the null results obtained by other groups since the lines-of-sight fall into a region with minimal reported variation.

It has to be noted that a large-scale spatial variation of this magnitude is not expected. It cannot be obtained easily in simplest theoretical models where varying fundamental couplings are due to dynamical scalar fields. One can nevertheless reproduce it by constructing toy models, for example as the result of domains formed at spontaneous breaking of a discrete symmetry of a dilaton-like scalar field coupled to electromagnetism (Olive et al. 2011). In any case, if such a result is confirmed, it will highlight the presence of currently unknown mechanisms which cause nature’s physical couplings to have different values in different regions of the universe. Observational and experimental confirmation or refutation of these results is therefore important. In addition to their intrinsic interest, these measurements (whether they are detections or null results) can shed light on the enigma of dark energy (Amendola et al. 2012).

One possible weakness in the evidence for variations in  $\alpha$  is that it derives from mostly ‘archival’ Keck and VLT spectra. In particular, the majority of the spectra analysed by King et al. (2012) were obtained in ‘service’ observing mode at the VLT. While spectroscopic quasar observations are generally straightforward, the ‘service’ calibration plan for most VLT/UVES observations only include wavelength calibration exposures of a thorium–argon (ThAr) lamp many hours after the relevant quasar exposures. This introduces the possibility of systematic mis-calibrations of the quasar wavelength scales. With this possibility in mind, and motivated by the need to confirm or refute current evidence for variations in  $\alpha$ , we are conducting ESO Large Program 185.A-0745, “*The UVES Large Program for testing Fundamental Physics*”. The aim is to obtain high signal-to-noise ratio ( $S/N \sim 100$  per pixel) spectra of  $\sim 12$  bright quasars, carefully selected to contain a total of  $\sim 25$  absorbers along their sight-lines in which  $\Delta\alpha/\alpha$  can be determined with precision bet-

ter than  $\sim 10$  ppm. In each quasar line-of-sight there exists at least one absorber in which we expect a precision approaching  $\sim 2$  ppm based on the variety of metal-line transitions available and the shape/structure of their absorption profiles.

In the present work we focus on the first line-of-sight from the Large Program: the bright quasar HE 2217–2818. This sight-line shows 5 separate absorption systems at redshifts 0.9–1.7 in which  $\alpha$ -sensitive transitions can be observed at high resolution with unusually high  $S/N$ . This line of sight subtends an angle of  $\Theta \approx 58^\circ$  with respect to the pole of the simplest model of dipolar variation in  $\alpha$  across the sky in King et al. (2012). The expected signal at this position on the sky is therefore  $\Delta\alpha/\alpha \approx +5.4$  ppm. Achieving a statistical precision in  $\Delta\alpha/\alpha$  of  $\lesssim 2$  ppm, as we aim to do in the  $z_{\text{abs}} = 1.6919$  absorber towards HE 2217–2818 in this paper using our new, high- $S/N$  observations, therefore contains a possibility of evidence for or against the dipolar model of spatial variation in  $\alpha$ . However, another major goal of studying this first quasar from the Large Program is to reveal systematic errors which may not randomize over the larger sample we will present in future papers. In particular, for the absorption system at  $z_{\text{abs}} = 1.6919$ , we present the results of two separate analyses to assist in the assessment of systematic effects.

## 2. Observations, data reduction and calibration

### 2.1. Observations

HE 2217–2818 is a relatively bright quasar with  $V \approx 16.0$  and with  $z_{\text{em}} = 2.46$ . Its spectrum shows several intervening systems at  $z_{\text{abs}} = 0.600, 0.7866, 0.9424, 1.054, 1.083, 1.200, 1.5558, 1.6279, 1.6919$  and  $2.181$ . However, only some of them, i.e. those detected in multiple transitions of the low-ionization ions Fe II, Si II and Mg II at  $z_{\text{abs}} = 0.7866, 0.9424, 1.5558, 1.6279$ , and  $1.6919$ , are suitable to probe the fine-structure constant. The other systems have metal lines which are either too weak or which fall in the Lyman forest short-ward of  $\approx 420$  nm.

The observations of HE 2217–2818 were performed with UVES on VLT on the nights of 13, 15, 16 and 17 June 2010, during the first visitor-mode run of observations for our Large Program. The journal of observations and relevant additional information is given in Table 1. The observations comprised 16 separate UVES exposures of  $\approx 4000$  s duration taken on five successive nights for a total of  $\approx 64000$  sec of integration. Half of the observations were taken with dichroic N. 2 with central wavelengths of the blue and red arm at 437 and 760 nm (setting 437+760). The other half were taken with the dichroic N. 1 in the 390+580 nm setting. These two wavelength settings overlap somewhat, and as a whole they provide almost complete spectral coverage from 350 up to 947 nm. The CCDs were set with no on-chip binning and the pixel size ranged between 0.013–0.015  $\text{\AA}$  pixel $^{-1}$ , or 1.12  $\text{km s}^{-1}$  pixel $^{-1}$  at 400 nm, along the dispersion direction. For all observations the slit-width was set to  $0.8''$  providing an instrumental line-spread function with a FWHM of  $\approx 3.57$  pixel in the 390 nm frames and  $\approx 4.38$  pixel in the 580 nm frame, with a variation of about 20% along the individual echelle orders. This corresponds to a resolving power of  $R \approx 55000$ . During the observations the seeing varied in the range between  $0.5''$  and  $1''$  as measured by the Differential Image Motion Monitor telescopes at Paranal Observatory. However, at the slightly higher and more protected location of VLT Unit Telescope 2 (on which UVES is mounted) the seeing was generally 10–30% better, as measured on the telescope guiding instrumentation.

**Table 1.** Journal of the observations of HE 2217–2818.

| Date       | UT       | $\lambda_c$ (nm) | Exp(sec) |
|------------|----------|------------------|----------|
| 2010-06-13 | 05:39:48 | 390              | 4000     |
| 2010-06-13 | 06:51:14 | 390              | 4000     |
| 2010-06-13 | 08:03:40 | 390              | 4000     |
| 2010-06-13 | 09:13:00 | 390              | 3600     |
| 2010-06-15 | 05:58:25 | 390              | 4000     |
| 2010-06-15 | 07:07:47 | 390              | 3767     |
| 2010-06-15 | 08:16:02 | 390              | 3767     |
| 2010-06-15 | 09:21:48 | 390              | 3767     |
| 2010-06-16 | 05:27:19 | 437              | 4020     |
| 2010-06-16 | 06:37:00 | 437              | 4020     |
| 2010-06-16 | 07:49:49 | 437              | 4000     |
| 2010-06-16 | 08:59:10 | 437              | 4020     |
| 2010-06-17 | 05:27:58 | 437              | 4000     |
| 2010-06-17 | 06:35:29 | 437              | 4000     |
| 2010-06-17 | 07:56:57 | 437              | 4000     |
| 2010-06-17 | 09:04:51 | 437              | 4000     |
| 2010-06-13 | 05:39:44 | 580              | 4000     |
| 2010-06-13 | 06:51:10 | 580              | 4000     |
| 2010-06-13 | 08:03:36 | 580              | 4000     |
| 2010-06-13 | 09:12:57 | 580              | 3600     |
| 2010-06-15 | 05:58:21 | 580              | 4000     |
| 2010-06-15 | 07:07:43 | 580              | 3767     |
| 2010-06-15 | 08:15:58 | 580              | 3767     |
| 2010-06-15 | 09:21:40 | 580              | 3767     |
| 2010-06-16 | 05:27:15 | 760              | 4020     |
| 2010-06-16 | 06:36:56 | 760              | 4020     |
| 2010-06-16 | 07:49:45 | 760              | 4000     |
| 2010-06-16 | 08:59:06 | 760              | 4020     |
| 2010-06-17 | 05:27:54 | 760              | 4000     |
| 2010-06-17 | 06:35:25 | 760              | 4000     |
| 2010-06-17 | 07:56:53 | 760              | 4000     |
| 2010-06-17 | 09:04:47 | 760              | 4000     |

## 2.2. Data reduction

We followed two independent approaches for the data reduction. Both analysis utilized the Common Pipeline Language version of the various tools constituting the UVES data reduction pipeline<sup>1</sup>. The pipeline first bias-corrects and flat-fields the quasar exposures. The echelle orders are curved and somewhat tilted with respect to the CCD rows/columns, so the pipeline locates them using an exposure of a quartz lamp observed through a pinhole instead of a standard slit. The quasar flux is then extracted with an optimal extraction method over the several pixels in the cross dispersion direction where the source flux is distributed. The wavelength calibration was performed using ThAr lamp exposures; it is a particularly important step for our purposes – see detailed discussion in Section 2.3 below. While the CPL code redisperses the spectra on to a linear wavelength scale by default, we used only the original, un-redispersed flux and error array for each echelle order in subsequent reduction steps. After wavelength calibration, the air wavelength scale of each echelle order, of each quasar exposure, was corrected from air to vacuum using the Edlén (1966) formula, and placed in the Solar System’s barycentric reference frame using the date and time of the mid-point of the exposure’s integration.

In the first analysis approach, the extracted flux from individual exposures was redispersed to a common linear wavelength grid and co-added with standard routines within the ESO MIDAS package using the S/N at the echelle order centres as weights. The quasar continuum was fitted in local regions around absorp-

tion lines with low-order polynomials. In the second analysis approach, a custom code, UVES\_POPLER<sup>2</sup> was used to redisperse the flux from individual exposures onto a common log-linear wavelength scale with dispersion  $1.3 \text{ km s}^{-1} \text{ pixel}^{-1}$ . The flux from all exposures was scaled to match that of overlapping orders and then co-added with inverse-variance weighting and cosmic ray rejection. UVES\_POPLER was also used to automatically fit a continuum to the final spectrum. This continuum was generally acceptable, though some local adjustments were made using low-order polynomial fits in the vicinity of some metal absorption lines.

## 2.3. Wavelength calibration

A variation of the  $\alpha$  should manifest itself as small radial velocity shifts between transitions. These transitions may fall hundreds of Ångströms, and many echelle order apart in the quasar spectrum. Since the signal for a non-zero  $\Delta\alpha/\alpha$  comes from the relative wavelength spacing of these transitions, having an accurate wavelength scale is crucial. The standard method used to calibrate the wavelength scale for a given science exposure with UVES is to take a hollow cathode ThAr arc lamp exposure with the same echelle and cross-disperser settings as the science exposure. Since December 2001, ESO has implemented an automatic resetting of the Cross Disperser encoder positions of UVES at the start of every image acquisition<sup>3</sup>. This policy was introduced to allow the use of day-time ThAr calibration frames to save on night-time calibration overheads. A negative aspect of this choice is that it implies that calibrations are taken under different conditions (e.g. ambient temperature, pressure, telescope pointing, telescope–instrument orientation differences etc.) from those prevailing during the quasar observations. It also implies that a ThAr exposure taken immediately before or after a quasar exposure may not accurately reflect the wavelength scale of the latter: the grating encoders are reset at each new acquisition sequence, so each time the quasar or ThAr arc is acquired for a subsequent exposure, the grating encoders, in principle, are moved.

One of the principal aims of our new observations is to avoid possible systematic effects introduced by this ‘service’ calibration plan. Therefore, ThAr exposures were taken before and after each quasar observation during the entire observing run, though only the ThAr frame taken after the quasar exposure was “attached” to the quasar exposure: this special mode allows us to avoid the automatic resets of grating positions between the quasar and calibration exposures. For this reason, the wavelength calibration of each quasar exposure studied in this paper was performed with its corresponding “attached” ThAr exposure. This procedure ensures that no mechanical movements occur between the quasar and ThAr frames and provides the best possible calibration for UVES.

The minimum and maximum temperatures during exposures within the spectrograph in correspondence to the blue arm’s CCD camera are monitored. During science exposures, typical changes are  $\Delta T \leq 0.1 \text{ K}$ , with two cases showing changes of 0.2 K. Ambient air pressure values are surveyed at the beginning and end of the exposures and reveal pressure changes of  $\Delta P = 0.2$  to 0.8 mbar. The impact of the temperature and pressure variations on UVES radial velocity stability are of  $50 \text{ m s}^{-1}$

<sup>1</sup> See [http://www.eso.org/observing/dfo/quality/UVES/pipeline/pipe\\_reduc.html](http://www.eso.org/observing/dfo/quality/UVES/pipeline/pipe_reduc.html).

<sup>2</sup> Written and maintained by MTM [http://astronomy.swin.edu.au/~mmurphy/UVES\\_popler](http://astronomy.swin.edu.au/~mmurphy/UVES_popler)

<sup>3</sup> See the UVES pipeline user manual p. 78

for  $\Delta T = 0.3$  K or  $\Delta P = 1$  mbar<sup>4</sup>. The measured values assure radial velocity stability within  $\approx 50$  m s<sup>-1</sup>. Of course, if such a spurious velocity shift were equally imparted to all transitions in a given spectrum, this would not result in a spurious shift in  $\Delta\alpha/\alpha$ ; only velocity shifts *between* transitions should affect a measured value of  $\Delta\alpha/\alpha$ . According to the Edlén (1966) formula for the refractive index of air, pressure and temperature changes of 0.1 K and 1 mbar would cause *differential* velocity shifts of  $\leq 15$  m s<sup>-1</sup> across the wavelength range of the spectrum studied here, implying a negligible effect on  $\Delta\alpha/\alpha$ .

The use of attached ThAr lamps, together with the use of no on-chip pixel binning, and a narrower spectrograph slit are the main differences with respect to most of the previous observations dealing with the search for the variability of fundamental physical constants using UVES.

In the first analysis approach, the wavelength calibration was established with the CPL pipeline’s standard method, i.e. extraction of the ThAr flux along the centre of each echelle order. In the second analysis approach, the ThAr flux was extracted using the object profile weights from its corresponding quasar exposure. The procedure for the selection of ThAr lines and the analysis leading to a wavelength solution follows that outlined in Murphy et al. (2007a). Specifically, in the 390 nm or 437 nm frames about 400 ThAr lines were identified, and more than 55% of them were used to calibrate the lamp exposures. A polynomial of the 5th order was adopted to match the selected lines. Residuals of the wavelength calibrations were typically of  $\approx 0.34$  mÅ, or  $\approx 24$  m s<sup>-1</sup> at 400 nm and symmetrically distributed at all wavelengths. We note that uncertainties of the laboratory wavelengths of individual thorium lines vary from about 15 m s<sup>-1</sup> up to more than 100 m s<sup>-1</sup> for the poorly known lines (Lovis & Pepe 2007; Murphy et al. 2007a).

#### 2.4. Slit effects

The optical paths of the ThAr and quasar light beams through the spectrograph are not identical and therefore there may be effects which cannot be traced by the ThAr calibrations. The most important one is the difference in the slit illumination between a point like source, such as a quasar, and the calibration lamp, which provides a relatively uniform illumination of the slit. Even when the point-like source is well centered into the slit, the precise position could vary slightly from one exposure to another, depending also on telescope guiding and tracking. In UVES, a 1'0 slit-width corresponds to  $\approx 7.5$  km s<sup>-1</sup> when projected onto the CCD. Therefore even a small shift of 0'01 in the centroid of the light is sufficient to induce a shift of  $\sim 100$  m s<sup>-1</sup> in the entire spectrum relative to its corresponding ThAr calibration exposure. Exposures taken at different times will in general show different radial velocity shifts due to this effect. Indeed, this effect has been measured by Wendt & Molaro (2012) by cross-correlating 15 UVES spectra of quasar Q0347–383. These spectra showed peak-to-peak excursions of up to  $\approx 800$  m s<sup>-1</sup> with an average deviation of 170 m s<sup>-1</sup>.

Such a ‘slit shift’ of all metal absorption lines by the same velocity in a single spectrum does not affect  $\Delta\alpha/\alpha$ . However, this effect becomes relevant when co-adding different exposures and when comparing, as it is for our observations, spectra obtained with different UVES settings: the mean slit shift will vary as a function of wavelength because of the different contributions from different settings at different wavelengths. This can pro-

duce a systematic effect in  $\Delta\alpha/\alpha$  if absorption lines from quite different wavelength regions are used. Also, small radial velocity shifts between exposures will produce a slight degradation of the S/N and effective instrumental line-shape in the final co-added spectrum. The desire to obtain co-added quasar spectra with high S/N precludes the use of individual quasar exposures for analysis because they usually have too low S/N. One exception was the very bright quasar HE 0515–4414, which provided one of the highest statistical precisions on  $\Delta\alpha/\alpha$  from an individual absorption system so far (Levshakov et al. 2005).

In our first analysis approach we measured the relative slit shifts of the individual quasar exposures by cross-correlating them with the mean spectrum. After selecting regions without telluric lines or ‘cosmic-ray’ features, we applied the XCSAO code from IRAF to cross-correlate the strongest absorption features. The two settings are summarized in Fig. 1. Despite the fact that relatively few features can be used for the purpose, global radial velocity shifts between different exposures were detected with high confidence. These slit shifts are typically of few hundred m s<sup>-1</sup> with a maximum amplitude of  $\approx 700$  m s<sup>-1</sup>, in agreement with Wendt & Molaro (2012).

The second analysis approach used a custom  $\chi^2$  minimization technique to compare each individual exposure with the mean spectrum (rather than a cross-correlation method). This method is described in detail by Evans & Murphy (2013). Its principle advantage for this application is that it does not require prior identification of ‘strong’ absorption features, instead utilizing all absorption features which contain enough ‘spectral information’ to provide a reliable shift measurement for each exposure. The slit shifts measured via this second approach are also shown in Fig. 1. In general there is very good agreement between the measurements from the two approaches, broadly consistent with the typical uncertainty of  $\sim 30$ – $80$  m s<sup>-1</sup>.

In Fig. 1 it is interesting to note that, in general, the shifts of the two different UVES arms of a given setting are comparable in amplitude and sign. This is expected in the case of good optical alignment of the two separate slits of the two UVES arms (blue and red). This is not obvious *a priori* because the two arms of the spectrograph have two different entrance slits and any optical misalignment will produce radial velocity differences between the two arms’ spectra. Molaro et al. (2008a) compared the radial velocity measured in the two arms using the sunlight reflected by an asteroid, and came to a similar conclusion. We note that with UVES, no telescope or instrument control is provided to control the relative slit alignment with the desirable accuracy, and the optical alignment can, in principle, change from one observing run to another.

In both analysis approaches, each exposure was corrected for the slit shifts discussed above. The 8 exposures were then combined in each setting separately to allow overlapping regions of neighboring settings to be compared using the same two approaches discussed above (cross-correlation and  $\chi^2$  minimization). This revealed residual velocity shifts, referred to as ‘setting shifts’ hereafter, between the 390 and 437-nm co-added spectra of  $-60 \pm 52$  and  $-93 \pm 38$  m s<sup>-1</sup> in the first and second analysis approaches, respectively. The settings shifts between the overlapping portions of the 580 and 760-nm co-added spectra were  $-7 \pm 48$  (first approach) and  $-155 \pm 43$  m s<sup>-1</sup> (second approach). Unfortunately, there are too few strong, particularly narrow absorption features in the small overlapping wavelength range ( $\sim 4800$ – $4950$  Å) between the 437 and 580-nm settings, so we cannot check the setting shifts between them with adequate precision. However, the previous results for the slit shifts between the two UVES arms discussed above provide evidence

<sup>4</sup> UV-Visual Echelle Spectrograph User Manual, 2004, <http://www.eso.org/instruments/uves/userman>.

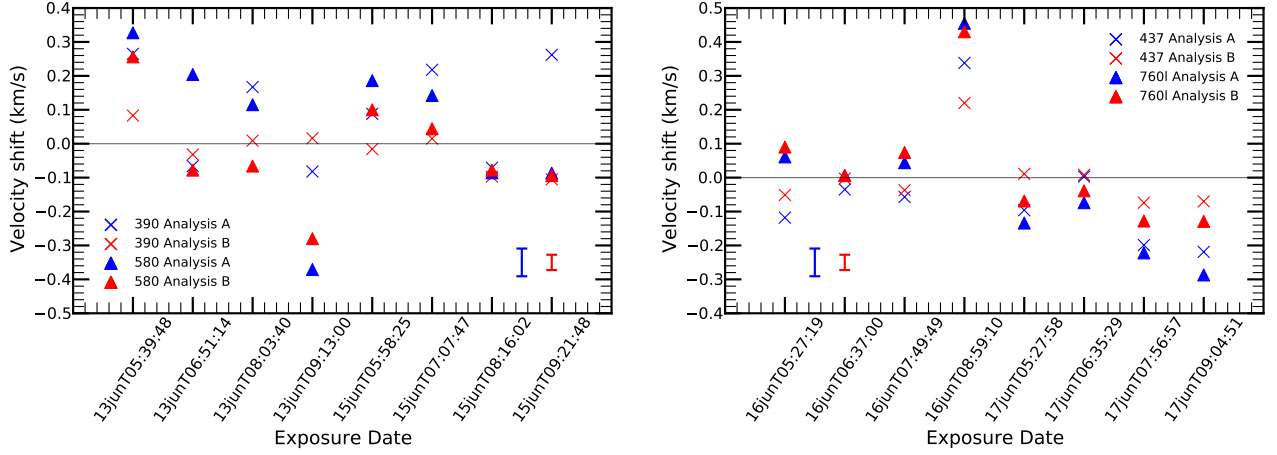


**Fig. 1.** Radial velocity ‘slit shifts’ between absorption lines in individual exposures and the same lines in the mean spectrum. Left panel: Shifts for the 390 nm (crosses) and 580 nm (triangles) settings. Right panel: Shifts for the 437 nm (crosses) and bluer chip of the 760 nm (triangles) settings. In both panels, blue points correspond to the first analysis approach and the red points correspond to the second analysis approach. Representative error bars for each analysis approach are shown in each panel.

that the shift between the 437 and 580-nm settings should be consistent with zero within  $\sim 30 \text{ m s}^{-1}$ . That is, we should expect the 390-vs-437-nm and 580-vs-760-nm setting shifts to be consistent with each other within each analysis approach, which we do observe. Indeed, for the second analysis approach, we adopted a single setting shift of  $-124 \pm 41 \text{ m s}^{-1}$  as representative of the 390-vs-437 and 580-vs-760-nm estimates. We should not expect large differences between the setting shifts of the two different approaches, and this also seems to be observed.

In both analysis approaches, the final spectrum (in which  $\Delta\alpha/\alpha$  is to be measured) was formed by co-adding the 8 exposures in all settings after removing the ‘slit shifts’ and ‘setting shifts’ from the individual exposures. These final spectra have a high S/N, with values up to  $\approx 100$  in the continuum in most of the spectral regions of interest. In Section 4.1.1 we consider the effect of not correcting for the slit and setting shifts.

### 2.5. Known systematic effects in the wavelength calibration

The possible presence of distortions in wavelength scales of Keck/HIRES spectra was investigated by Griest et al. (2010) by comparing the ThAr wavelength scale with that established from I2-cell observations. In the wavelength range  $\sim 5000\text{--}6200 \text{ \AA}$  covered by the iodine cell absorptions they found a saw-tooth distortion pattern with amplitude of typically  $300 \text{ m s}^{-1}$  along each echelle order. The distortions are such that transitions at the order edges appear at different velocities with respect to transitions at the order centers when the two calibrations are compared. Whitmore et al. (2010) repeated the same test for UVES and found similar effects, though the saw-tooth distortion shows reduced peak-to-peak velocity variations of  $\sim 200 \text{ m s}^{-1}$ . The origin of these distortion is not clear. Wilken et al. (2010) on spectra obtained with the HARPS spectrograph at the 3.6m ESO telescope on La Silla, and calibrated by means of a Laser Frequency Comb detected very small differences in the size of physical pixels due to CCD manufacturing. In general, an individual CCD sensor is built up by means of several unit cells or blocks which are connected to each other during the design or lay-out phase of the development cycle of the sensor. The block stitching process could produce misalignments between different CCD blocks of the order of  $\sim 10^{-2}$  of the pixel size. The calibration polynomial

cannot cope with these sudden changes in the dispersion solution and oscillates to accommodate it. This ‘‘overcompensation’’ will produce local calibration distortions. Since blocks have typical sizes of 512 pixels, or  $\approx 13 \text{ \AA}$  in UVES, shifts could occur even for neighboring absorption lines, such as the Mg II doublet, or even within a single absorption profile where the components span several hundreds  $\text{km s}^{-1}$  and may fall over two different CCD manufacturing blocks. We test for systematic errors of this kind in Section 4.1.1.

We note that Molaro et al. (2011) compared solar features observed both with HARPS and UVES and found such ‘intra-order distortions’ in the UVES spectrum with a typical scale of  $\approx 10 \text{ \AA}$ . In HARPS the offsets were measured up to  $50 \text{ m s}^{-1}$  within one order and in UVES, where the pixel size is a factor 3 bigger, the offsets could be a factor 3 larger. We note also that the  $\pm 40 \text{ m s}^{-1}$  inaccuracies of the HARPS wavelength scale revealed by the Laser Frequency Comb test contribute to the line-list constructed for use with UVES (Lovis & Pepe 2007; Murphy et al. 2007a).

## 3. Many-Multiplet method and Fitting

### 3.1. Many-Multiplet method

The change in the rest-frame frequencies between the laboratory,  $\omega_i(0)$ , and in an absorber at redshift  $z$ ,  $\omega_i(z)$ , due to a small variation in  $\alpha$ , i.e.  $\Delta\alpha/\alpha \ll 1$ , is proportional to a  $q$ -coefficient for that transition:

$$\omega_i(z) \equiv \omega_i(0) + q_i \left[ (\alpha_z/\alpha_0)^2 - 1 \right], \quad (1)$$

where  $\alpha_0$  and  $\alpha_z$  are the laboratory and absorber values of  $\alpha$ , respectively (Dzuba et al. 1999). The  $q$ -coefficients for the transitions of interest are given in the last column of Table 2. The change in frequency is observable as a velocity shift,  $\Delta v_i$ , of transition  $i$ .

$$\frac{\Delta v_i}{c} \approx -2 \frac{\Delta\alpha}{\alpha} \frac{q_i}{\omega_i(0)}. \quad (2)$$

The MM method is based on the comparison of measured velocity shifts from several transitions having different  $q$ -coefficients to compute the best-fitting  $\Delta\alpha/\alpha$ .

When applied across a variety of different ionic species (i.e. different atoms or ionization stages of the same atom), the MM method assumes that the different species traces the same material, or at least that there are no substantial intrinsic velocity shifts between the absorption lines of different species. Therefore, to reduce the number of free parameters in a fit to all transitions of all species, we impose the requirement that corresponding fitted velocity components in different species share the same overall redshifts (i.e. cosmological redshift and peculiar velocity combined). Unless there is evidence for the lines being thermally broadened, we also assume that the lines are broadened by macro-turbulence motions. That is, we assume that corresponding velocity components in different species have the same fitted Doppler broadening parameter.

The laboratory atomic parameters used in our analyses – rest-frame frequencies, oscillatory strengths etc. – were taken from a new compilation (Murphy & Berengut, in prep.), the important details of which are not significantly different from that used by King et al. (2012). These are reported in Table 2. In particular, the laboratory wavelength for the Fe II  $\lambda 1608$  transition was taken from Nave & Sansonetti (2011). The isotopic structures of most transitions are also reported, together with the composite laboratory wavelength expected for a solar isotopic composition.

### 3.2. Selection of transitions

To build the best model of the velocity structure of an absorption system, we try to include as many different transitions as possible. However, the presence of contaminating absorption lines could strongly skew the analysis, so we did not include transitions that were blended with absorption features of other systems at other redshifts. For the two different analysis approaches we took two approaches to deal with sky (telluric) lines. The first approach was to remove the regions affected by the telluric lines if their presence could be established based on the spectrum itself, or through comparison with a standard star spectrum taken during our observations. The second approach was more conservative, completely rejecting transitions which had any possible telluric line contamination, even if only in a small part of the velocity structure of the transition. Finally, in neither approach did we consider any transitions which fall in the Ly $\alpha$  forest portion of the spectrum for the analysis of  $\Delta\alpha/\alpha$ , even if part of their velocity structure presented no evidence of contamination by broad Ly $\alpha$  lines.

### 3.3. Absorption-line fitting

The model fitting of the absorption profile is performed by means of the non-linear least squares Voigt profile fitting program VPFIT by Bob Carswell and John Webb<sup>5</sup>. This code has been widely used for the absorption line analysis and has been modified to incorporate  $\alpha$  as a free parameter in the fit (Murphy et al. 2003). For a given transition to be fitted, the model is specified by defining the number of components, the spectral region on which the fitting is performed and the instrumental profile. The analysis in both approaches proceeds in two basic steps. The first one consists in obtaining a fiducial model for the absorption while keeping  $\Delta\alpha/\alpha$  fixed at zero. That is, the number of velocity components and their distribution across the absorption complex, is refined without any influence on or from a varying

**Table 2.** Laboratory atomic data for the transitions used in our analyses, taken from Murphy & Berengut (in prep.; see also King et al. 2012). The third column shows the oscillator strength or, in the case of an isotopic or hyperfine structure component, the terrestrial isotopic abundance fraction or the relative hyperfine level population (in local thermodynamic equilibrium). An asterisk (\*) indicates information taken from Nave & Sansonetti (2011).

| Ion                      | $\lambda_0$<br>[Å] | $f$ or % | $q$<br>[cm <sup>-1</sup> ] |
|--------------------------|--------------------|----------|----------------------------|
| Mg I 2852                | 2852.962797(15)    | 1.83     | 86(10)                     |
| <sup>26</sup> Mg I 2852  | 2852.959591(20)    | 11.0%    |                            |
| <sup>25</sup> Mg I 2852  | 2852.961407(20)    | 10.0%    |                            |
| <sup>24</sup> Mg I 2852  | 2852.963420(14)    | 79.0%    |                            |
| Mg II 2796               | 2796.353794(16)    | 0.6155   | 211(10)                    |
| <sup>26</sup> Mg II 2796 | 2796.3470457(4)    | 11%      |                            |
| <sup>25</sup> Mg II 2796 | 2796.348269(50)    | 4.2%     |                            |
| <sup>25</sup> Mg II 2796 | 2796.352784(50)    | 5.8%     |                            |
| <sup>24</sup> Mg II 2796 | 2796.3550990(4)    | 79.0%    |                            |
| Mg II 2803               | 2803.530983(16)    | 0.3058   | 120(2)                     |
| <sup>26</sup> Mg II 2803 | 2803.5242094(4)    | 11%      |                            |
| <sup>25</sup> Mg II 2803 | 2803.525314(50)    | 4.2%     |                            |
| <sup>25</sup> Mg II 2803 | 2803.530004(50)    | 5.8%     |                            |
| <sup>24</sup> Mg II 2803 | 2803.5322972(4)    | 79.0%    |                            |
| Al II 1670               | 1670.78861(11)     | 1.74     | 270(30)                    |
| Al III 1854              | 1854.717941(34)    | 0.559    | 464(30)                    |
| <i>F</i> =2              | 1854.708966(28)    | 41.7     |                            |
| <i>F</i> =3              | 1854.724704(21)    | 58.3     |                            |
| Al III 1862              | 1862.791127(69)    | 0.278    | 216(30)                    |
| <i>F</i> =2              | 1862.780325(52)    | 41.7     |                            |
| <i>F</i> =3              | 1862.798581(42)    | 58.3     |                            |
| Si II 1526               | 1526.706980(16)    | 0.133    | 50(30)                     |
| <sup>30</sup> Si II 1526 | 1526.7072550       | 3.1%     |                            |
| <sup>29</sup> Si II 1526 | 1526.7071150       | 4.7%     |                            |
| <sup>28</sup> Si II 1526 | 1526.7069637       | 92.2%    |                            |
| Fe II 1608               | 1608.45081(7)*     | 0.0577   | -1299(300)                 |
| <sup>58</sup> Fe II 1608 | 1608.4519539       | 0.3%     |                            |
| <sup>57</sup> Fe II 1608 | 1608.4514182       | 2.1%     |                            |
| <sup>56</sup> Fe II 1608 | 1608.4508635       | 91.8%    |                            |
| <sup>54</sup> Fe II 1608 | 1608.4496923       | 5.8%     |                            |
| Fe II 2344               | 2344.212747(76)    | 0.114    | 1210(150)                  |
| <sup>58</sup> Fe II 2344 | 2344.2113616       | 0.3%     |                            |
| <sup>57</sup> Fe II 2344 | 2344.2120103       | 2.1%     |                            |
| <sup>56</sup> Fe II 2344 | 2344.2126822       | 91.8%    |                            |
| <sup>54</sup> Fe II 2344 | 2344.2141007       | 5.8%     |                            |
| Fe II 2374               | 2374.460064(78)    | 0.0313   | 1590(150)                  |
| <sup>58</sup> Fe II 2374 | 2374.4582998       | 0.3%     |                            |
| <sup>57</sup> Fe II 2374 | 2374.4591258       | 2.1%     |                            |
| <sup>56</sup> Fe II 2374 | 2374.4599813       | 91.8%    |                            |
| <sup>54</sup> Fe II 2374 | 2374.4617873       | 5.8%     |                            |
| Fe II 2382               | 2382.763995(80)    | 0.320    | 1460(150)                  |
| <sup>58</sup> Fe II 2382 | 2382.7622294       | 0.3%     |                            |
| <sup>57</sup> Fe II 2382 | 2382.7630560       | 2.1%     |                            |
| <sup>56</sup> Fe II 2382 | 2382.7639122       | 91.8%    |                            |
| <sup>54</sup> Fe II 2382 | 2382.7657196       | 5.8%     |                            |
| Fe II 2586               | 2586.649312(87)    | 0.0691   | 1490(150)                  |
| <sup>58</sup> Fe II 2586 | 2586.6475648       | 0.3%     |                            |
| <sup>57</sup> Fe II 2586 | 2586.6483830       | 2.1%     |                            |
| <sup>56</sup> Fe II 2586 | 2586.6492304       | 91.8%    |                            |
| <sup>54</sup> Fe II 2586 | 2586.6510194       | 5.8%     |                            |
| Fe II 2600               | 2600.172114(88)    | 0.239    | 1330(150)                  |
| <sup>58</sup> Fe II 2600 | 2600.1703603       | 0.3%     |                            |
| <sup>57</sup> Fe II 2600 | 2600.1711816       | 2.1%     |                            |
| <sup>56</sup> Fe II 2600 | 2600.1720322       | 91.8%    |                            |
| <sup>54</sup> Fe II 2600 | 2600.1738281       | 5.8%     |                            |

<sup>5</sup> The 9.5 version of the VPFIT manual is available at <ftp://ftp.ast.cam.ac.uk/pub/rfc/vpfit9.5.pdf>

$\Delta\alpha/\alpha$  parameter. Once the model for the absorption is derived, giving a satisfactory fit of the data with all residuals consistent with the error arrays,  $\Delta\alpha/\alpha$  is introduced as a new free parameter to provide a better fit to the data.

The statistical uncertainty in  $\Delta\alpha/\alpha$  is determined from the relevant diagonal term of the covariance matrix of the best-fitting solution. This is multiplied by  $\sqrt{\chi^2_\nu}$ , where  $\chi^2_\nu$  is the  $\chi^2$  between the model and data per degree of freedom,  $\nu$ , to yield more reliable uncertainties (Press et al. 1992). The accuracy and reliability of these statistical uncertainties has been confirmed with detailed Monte Carlo and also Monte Carlo Markov Chain simulations (King et al. 2009; Murphy 2002). This approach is successful because the covariance between the  $\Delta\alpha/\alpha$  parameter and other parameters in the fit is minimal. However, this is not always true for parameters of individual components in the fit. In particular, the column density and Doppler broadening parameters of an individual component are covariant, and strongly covariant with those parameters of close-blended neighboring components. In the final absorption profile models presented in Tables 4–8, and described in the following sections, we present only statistical uncertainties derived from the diagonal terms of the covariance matrix for parameters of individual components.

Finally, during the fitting process, we set a lower limit on the Doppler parameter for individual components of  $b = 0.5 \text{ km s}^{-1}$ , which is well below the FWHM resolution of the spectra ( $\sim 5.5 \text{ km s}^{-1}$ ). These unresolved components generally have formal uncertainties (quoted in Tables 4–8) exceeding  $0.5 \text{ km s}^{-1}$ . In these cases, and for other components with  $b$ -parameters uncertainties exceeding their best-fitted value, it should be recognized that, while  $b$  is formally consistent with zero, this does not indicate that the component is redundant in the fit.

### 3.4. Instrument profile

The full-width-at-half-maximum (FWHM) of the instrumental profile of UVES varies by  $\approx 20\%$  along every echelle order due to the spectrograph anamorphosis. Therefore, the FWHM was computed by averaging the width of unblended thorium emission lines in the wavelength region around the metal absorption lines used to derive  $\Delta\alpha/\alpha$ . That is, the FWHM was calculated separately for each transition. Moreover, it is known that the FWHM of ThAr lines produced by a fully-illuminated slit is slightly broader than that produced by a point source which under-fills the slit. Simple models suggest that, even with FWHM seeing equivalent to the slit-width, the reduction in the FWHM resolution is  $\approx 10\%$ . The values used in the present analysis are those given in Table 3 reduced by 10%.

## 4. Analysis of absorption systems

We present below the analysis of the 5 absorption systems towards HE 2217–2818 in which we can measure  $\Delta\alpha/\alpha$ . We focus first on the highest-redshift absorber, that at  $z_{\text{abs}} = 1.6919$ , because this provides by-far the highest statistical precision on  $\Delta\alpha/\alpha$  and, therefore, requires the most comprehensive analysis and consideration of underlying systematic errors. We therefore describe in detail our two different analysis approaches for this system. For the other absorbers, we do not present all details of systematic error checks because the statistical uncertainty dominates the total error budget; we present only the results one analysis approach (the second) for simplicity.

### 4.1. Absorption system at $z_{\text{abs}} = 1.6919$

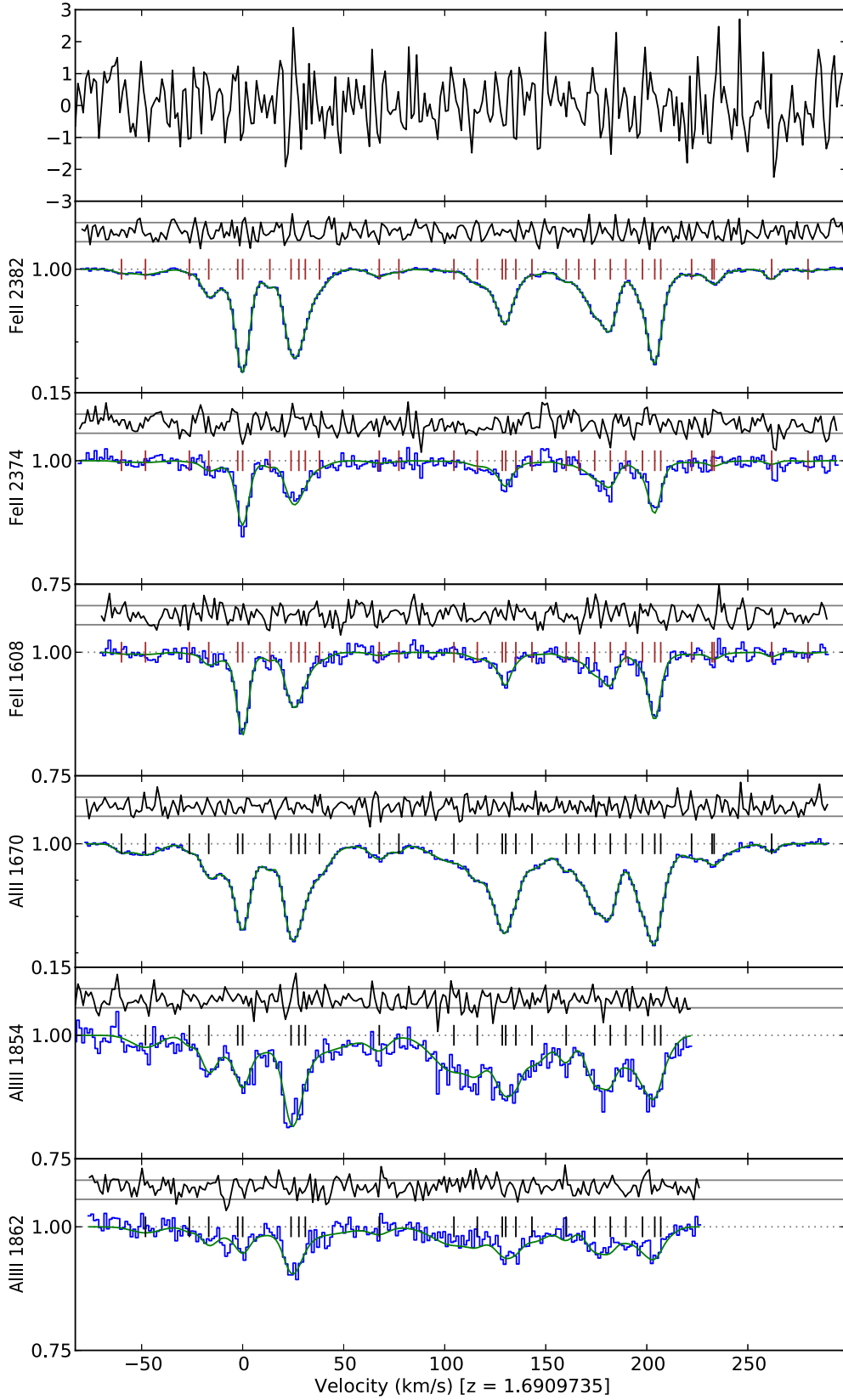
The system at redshift  $z_{\text{abs}} = 1.6919$  shows a quite complex velocity structure with many separate strong, narrow features spread over  $\sim 250 \text{ km s}^{-1}$ . The transitions observed red-wards of the Ly $\alpha$  forest in our spectral range, and which are potentially useful for measuring  $\Delta\alpha/\alpha$  are Al II  $\lambda\lambda 1670, 1862$ , Mg II  $\lambda\lambda 2796$  and Fe II  $\lambda\lambda 1608, 2344, 2374, 2382, 2586, 2600$ . Unfortunately, the detected Mg II  $\lambda 2796$  transition cannot be used because partially contaminated by a strong sky emission at  $\approx 7526.8 \text{ \AA}$ . The Mg II  $\lambda 2803$  and Mg I  $\lambda 2852$  transitions were not detected because they fall into the gap between the two red-arm CCDs in the 760-nm setting. The subset of these transitions used to constrain  $\Delta\alpha/\alpha$  in the second analysis approach is shown in Fig. 2.

Figure 2 shows that the velocity structure and relative strength of the different features is very similar in all the low-ionization transitions. The Al III  $\lambda\lambda 1854/1862$  doublet is not observed with high S/N and is not particularly strong. As a higher ionization species than the other transitions, including it in the analysis may introduce a stronger sensitivity to possible ionization differences between species. However, no evidence for differences in velocity structure are evident in Fig. 2, even though the relative strength of some features differs from the lower-ionization transitions. In general, some features are quite weak even in the stronger transitions and so they are not detectable in the weaker transitions. Note that, even by cursory visual inspection, it is clear that the stronger features are not symmetric and particularly narrow (unresolved); instead, their breadth and asymmetries reveal unresolved complex velocity structure.

Careful inspection of the spectrum of a fast rotating star allowed us to precisely identify the position of telluric features. The Fe II  $\lambda 2344$ , Fe II  $\lambda 2586$  and Fe II  $\lambda 2600$  all fall in a spectral region affected by telluric lines. Removing telluric absorption features is quite a difficult task because they vary with the physical conditions of the Earth’s atmosphere, thereby introducing time and line-of-sight dependencies. We did not attempt a correction but instead we adopted two different approaches to deal with this.

In the first analysis approach we excluded the spectral portions around the telluric lines in these transitions but we included the remaining portions in the  $\Delta\alpha/\alpha$  analysis. For Fe II  $\lambda 2344$  we considered only the intervals 6310.5–6311.5 and 6312.25–6312.7 Å. For Fe II  $\lambda 2586$  we considered only the intervals 6959.6–6961.5 and 6964.4–6965.75 Å and for Fe II  $\lambda 2600$  the intervals 6996.7–7000.5 and 7001.55–7002.79 Å. Our second analysis approach only considers the transitions which are not affected by telluric or any other contaminating lines. These are the three Fe II transitions  $\lambda\lambda 1608, 2374, 2382$ , the Al II  $\lambda 1670$  transition and the Al III  $\lambda\lambda 1854/1862$  doublet, as shown in Fig. 2.

The models of the absorption profiles were built up, step-by-step, by adding components at different velocities in all fitted species simultaneously and minimizing  $\chi^2$  at each step with  $\Delta\alpha/\alpha$  fixed at zero. The absorber’s velocity structure is quite complex and our first and second analysis approaches used 30 and 32 velocity components, respectively, to obtain statistically acceptable fits with  $\chi^2$  per degree of freedom,  $\chi^2_\nu \approx 1$ . This large number of velocity components is consistent the aforementioned characteristics of the profile: the five main features all show asymmetries and require at least 2 or 3 components each to adequately fit them. Additional components are needed to account for weak absorption between these main features; the need for these components is clear from inspection of the line pro-



**Fig. 2.** Transitions in absorption system at  $z_{\text{abs}} = 1.6919$  used to derive  $\Delta\alpha/\alpha$  in our second analysis approach. The Voigt profile model (green line) is plotted over the data (blue histogram). The velocity of each fitted component is marked with a vertical line and the residuals between the data and model, normalised by the error spectrum, are shown above each transition. The top panel shows the composite residual spectrum – the mean spectrum of the normalised residuals for all transitions shown – in units of  $\sigma$ .

**Table 3.** Local FWHM of the instrumental profile and local S/N measured in the continuum around each transition for all 5 absorbers studied here.

| Ion        | $z_{\text{abs}}=1.6919$ |                               | $z_{\text{abs}}=1.6279$ |                               | $z_{\text{abs}}=1.5558$ |                               | $z_{\text{abs}}=0.94$ |                               | $z_{\text{abs}}=0.7866$ |                               |
|------------|-------------------------|-------------------------------|-------------------------|-------------------------------|-------------------------|-------------------------------|-----------------------|-------------------------------|-------------------------|-------------------------------|
|            | S/N                     | FWHM<br>[km s <sup>-1</sup> ] | S/N                     | FWHM<br>[km s <sup>-1</sup> ] | S/N                     | FWHM<br>[km s <sup>-1</sup> ] | S/N                   | FWHM<br>[km s <sup>-1</sup> ] | S/N                     | FWHM<br>[km s <sup>-1</sup> ] |
| Fe II 1608 | 98                      | 5.22                          |                         |                               |                         |                               |                       |                               |                         |                               |
| Fe II 2344 | 117                     | 5.51                          | 110                     | 5.99                          | 121                     | 5.61                          |                       |                               |                         |                               |
| Fe II 2374 | 103                     | 5.82                          |                         |                               |                         |                               |                       |                               |                         |                               |
| Fe II 2383 | 130                     | 5.75                          | 113                     | 5.70                          | 124                     | 5.81                          | 88                    | 5.38                          | 106                     | 5.21                          |
| Fe II 2600 | 88                      | 5.43                          | 84                      | 5.40                          | 84                      | 5.87                          | 71                    | 6.06                          | 73                      | 5.38                          |
| Si II 1526 | 152                     | 5.24                          | 85                      | 5.35                          | 60                      | 5.35                          |                       |                               |                         |                               |
| Al II 1670 | 77                      | 5.50                          | 78                      | 5.21                          | 100                     | 5.34                          |                       |                               |                         |                               |
| Mg II 2796 | 78                      | 5.22                          | 96                      | 5.42                          | 97                      | 5.42                          | 53                    | 5.97                          | 65                      | 5.58                          |
| Mg II 2803 |                         |                               | 73                      | 5.42                          | 77                      | 5.42                          | 51                    | 5.95                          | 65                      | 5.58                          |

files of the optically thick transitions. We note that these weak components do not influence the value of  $\Delta\alpha/\alpha$  significantly. The first analysis approach excluded two of these components, i.e. the first approach represents a ‘minimally complex’ model. Conversely, the second approach required that the chosen model was that which minimized  $\chi^2_{\nu}$ . The 32-component model is provided in Table 4, with the final  $\chi^2_{\nu} = 1.20$ .

After the number and nominal relative velocities of the fitted components are finalised,  $\Delta\alpha/\alpha$  is introduced as an additional free parameter and determined, along with all other free parameters, in the  $\chi^2$  process. The two analysis approaches give the following best-fit values and 1- $\sigma$  statistical uncertainties for  $\Delta\alpha/\alpha$ :

$$\Delta\alpha/\alpha = \begin{cases} -3.8 \pm 2.1_{\text{stat}} \text{ ppm} & (\text{first approach}), \\ +1.3 \pm 2.4_{\text{stat}} \text{ ppm} & (\text{second approach}). \end{cases} \quad (3)$$

The main constraints on  $\Delta\alpha/\alpha$  are contributed by the combination of the high S/N transitions with diverse  $q$ -coefficients, i.e. those of Al II and Fe II, particularly the Fe II  $\lambda 1608$  transition which has a  $q$ -coefficient with opposite sign to the others. The results from the two analysis approaches in equation (3) appear at first to be rather inconsistent. This may indicate that important systematic errors are present in the calibration and analysis steps, since these constitute the main difference between the two approaches. To explore possible systematic errors in more details in Section 4.1.1 below.

One notable difference between the two analysis approaches is that the first includes 6 Fe II transitions, or parts thereof (after masking of telluric features), thereby making an analysis using just those transitions feasible. Using just one ionic species alleviates the possibility that ionization effects may systematically affect  $\Delta\alpha/\alpha$  (e.g. Levshakov et al. 2005). Of course, in the case of Fe II, the precision and accuracy of the result depend heavily on the Fe II  $\lambda 1608$  transition and any possible systematic errors applying to the data or wavelength calibration relevant to it. To conduct this Fe-only test, we restricted the region analyzed in each transition to the velocity range  $-35$  to  $+250$  km s<sup>-1</sup> in Fig. 2. This effectively removed the 2 velocity components in the model for the first approach corresponding to the weak features at the blue and red flanks of the absorber. A further 2 velocity components from that model were discarded as unnecessary by VPFIT because the high S/N Al II  $\lambda 1670$  transition had been removed. This left the model with 26 components. Furthermore, we derived  $\Delta\alpha/\alpha$  on an different reduction of the spectrum, with a slightly different binning and exposure combination approach to those presented above. The result based on this Fe-only analysis is  $\Delta\alpha/\alpha = +1.14 \pm 2.58_{\text{stat}}$  ppm. The difference between this result and that from the first approach in equation (3) demon-

strates that systematic effects may play an important role in the total uncertainty in  $\Delta\alpha/\alpha$ . We turn to quantifying the systematic error budget for this absorber below.

#### 4.1.1. Systematic error tests

We ran a number of tests on the second analysis approach to uncover the sensitivity of the result to various systematic effects. For each of these tests, we find the maximum deviation between the second approach’s  $\Delta\alpha/\alpha$  value in equation (3) and that given by the test, adding the results in quadrature to estimate the total systematic error budget.

Firstly, to test the convergence of the fitting procedure, we restarted the  $\chi^2$  minimization from its final solution but with starting values of  $\Delta\alpha/\alpha$  set to  $+1\sigma$  and  $-1\sigma$  away from its fiducial value. Both these test fits converged to  $\Delta\alpha/\alpha$  values very close to that in equation (3). The largest difference was 0.03 ppm, which we added in quadrature to the total systematic error budget.

The second test investigated the effect that co-adding the individual exposures into a final spectrum has on the absorption line centroids and, therefore,  $\Delta\alpha/\alpha$ . The software used to combine the spectra in the second analysis approach, UVES\_POPLER, first redisperses all echelle orders, from all exposures, onto a common wavelength scale with a constant pixel size in velocity space. A dispersion of  $1.30$  km s<sup>-1</sup> pixel<sup>-1</sup> was used for the final spectrum. To test the effect of redispersing and co-adding the individual exposures, we produced four new co-added spectra with slightly different dispersion values – 1.28, 1.29, 1.31 and  $1.32$  km s<sup>-1</sup> pixel<sup>-1</sup> – which ensures that the pixel grids will be very different for each transition from spectrum to spectrum. The values of  $\Delta\alpha/\alpha$  for these four different spectra varied by at most 0.54 ppm, and this was added in quadrature to the total systematic error budget.

The third test quantified the possible effect the ‘intra-order’ distortions of the UVES wavelength scale found by Whitmore et al. (2010) may have on  $\Delta\alpha/\alpha$ . For each echelle order, of each exposure, we applied a saw-tooth distortion to the existing wavelength scale and then co-added them in the usual way. The distortion applied had a peak-to-peak amplitude of  $200$  m s<sup>-1</sup>, varying from  $-100$  m s<sup>-1</sup> at the order edges to  $+100$  m s<sup>-1</sup> and the order centres. We also produced a second distorted spectrum where this saw-tooth pattern was reversed. Of course, we cannot be sure that the effect identified by Whitmore et al. (2010) is present in our spectra, or that it has the same pattern or magnitude in our spectra, but the two distorted spectra produced in this way allow us to gauge the size of the effect on  $\Delta\alpha/\alpha$ . Refitting for  $\Delta\alpha/\alpha$  on

these distorted spectra gives a maximum deviation between the distorted and fiducial results of 0.56 ppm.

The final test was aimed at understanding the effect that the ‘slit shifts’ and ‘setting shifts’ discussed in Sec. 2.4 have on  $\Delta\alpha/\alpha$ . The most straightforward test is to determine  $\Delta\alpha/\alpha$  using spectra in which these corrections have *not* been applied in the second analysis approach. Unsurprisingly, not applying the setting shift ( $-124 \pm 41 \text{ m s}^{-1}$ ) produces largest difference in  $\Delta\alpha/\alpha$ , 1.2 ppm, thus demonstrating that, were these effects not corrected, they would have caused a significant systematic error, about 50% of the statistical error. However, while we have corrected for these effects, we can not have done so perfectly, and errors in our corrections will propagate as systematic errors in  $\Delta\alpha/\alpha$ . The relative uncertainty on the setting shift is 33%, so we expect that the residual systematic error in this case is of order 0.4 ppm.

After adding the above estimates of the systematic error in quadrature, the total systematic error budget is 0.96 ppm. That is, the final result from the second analysis approach is

$$\Delta\alpha/\alpha = +1.3 \pm 2.4_{\text{stat}} \pm 1.0_{\text{sys}} \text{ ppm}. \quad (4)$$

#### 4.2. Absorption system at $z_{\text{abs}} = 1.6279$

The transitions used to constrain  $\Delta\alpha/\alpha$  in the second analysis approach for the absorption system at  $z_{\text{abs}} = 1.6279$  are shown in Fig. 3. The absorption profile model parameters from this approach are provided in Table 5. The absorption spans  $\sim 100 \text{ km s}^{-1}$  with three main features which are rather broad and very asymmetric, revealing a quite complex underlying velocity structure. Detected transitions not used to constrain  $\Delta\alpha/\alpha$  include strong Si II  $\lambda 1526$  absorption which falls in the Ly $\alpha$  forest.

The broad and multi-component nature of the 3 main absorption features translates to large statistical uncertainties on the redshifts of the velocity components and, therefore,  $\Delta\alpha/\alpha$ . The systematic error budget was determined by conducting the same systematic error tests as conducted on the  $z_{\text{abs}} = 1.6919$  absorber in Section 4.1.1. The final result for this  $z_{\text{abs}} = 1.6279$  absorber is then

$$\Delta\alpha/\alpha = +37.2 \pm 20.6_{\text{stat}} \pm 39.4_{\text{sys}} \text{ ppm}. \quad (5)$$

#### 4.3. Absorption system at $z_{\text{abs}} = 1.5558$

The transitions used to constrain  $\Delta\alpha/\alpha$  in the second analysis approach for the absorption system at  $z_{\text{abs}} = 1.5558$  are shown in Fig. 4. The absorption profile model parameters from this approach are provided in Table 6. The absorption spans  $\sim 100 \text{ km s}^{-1}$  with three main features which appear at first to be rather symmetric and narrower than the three features in the  $z_{\text{abs}} = 1.6279$  absorber. Indeed, the underlying velocity structure of these three features appears to be dominated by a single strong component in each case. However, our detailed approach to fitting all the *statistically required* velocity components reveals that several weaker components are required for an adequate fit. These are required for the higher optical depth transitions of Mg II  $\lambda 2796$  and Al II  $\lambda 1670$ . There are three telluric features which contaminate the Mg II  $\lambda 2803$ , so this is excluded from the analysis.

The  $\chi^2$  minimization analysis of the  $z_{\text{abs}} = 1.5558$  profiles shown in Fig. 4 and the systematic error tests conducted in Section 4.1.1 provide a final result of

$$\Delta\alpha/\alpha = -0.2 \pm 24.9_{\text{stat}} \pm 3.6_{\text{sys}} \text{ ppm}. \quad (6)$$

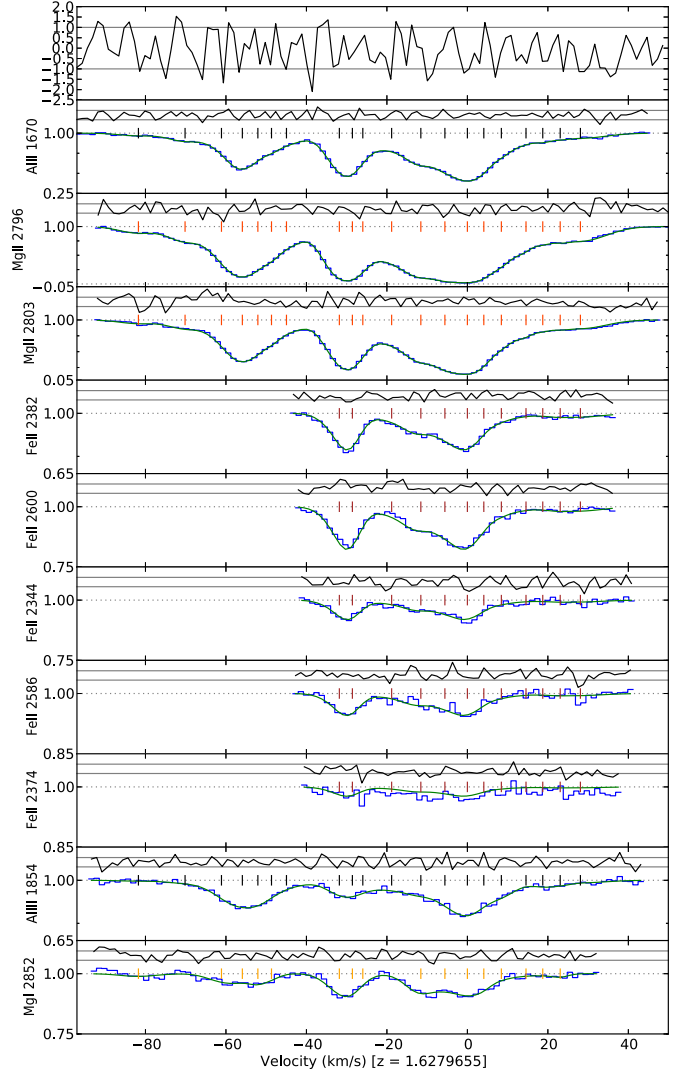


**Fig. 3.** Absorption profile for system at  $z_{\text{abs}} = 1.6279$  with transitions used in the second analysis approach for determining  $\Delta\alpha/\alpha$ . The figure is structured as in Fig. 2. Details of the absorption profile fit are given in Table 5.

Given the relatively large statistical uncertainty on  $\Delta\alpha/\alpha$  in this absorber, we neglect here the systematic error budget because it will be much smaller.

#### 4.4. Absorption systems at $z_{\text{abs}} = 0.9407$ and $0.9424$

The absorption around  $z_{\text{abs}} = 0.941$  comprises two absorption complexes, one with the main absorption at  $z_{\text{abs}} = 0.9407$  and the second with the strongest absorption at  $z_{\text{abs}} = 0.9424$ . They are separated by  $\sim 300 \text{ km s}^{-1}$  without any hint of absorption in any of the strongest detected transitions. Hence we fit them separately. The transitions used to constrain  $\Delta\alpha/\alpha$  in the second analysis approach for these systems are shown in Figs. 5 & 6. The absorption profile model parameters from this approach are provided in Table 7.

The absorption at  $z_{\text{abs}} = 0.9407$  spans  $\sim 100 \text{ km s}^{-1}$  and that at  $z_{\text{abs}} = 0.9424$  spans  $\sim 180 \text{ km s}^{-1}$  in the strongest transition, Mg II  $\lambda 2796$ . The first system comprises two well-separated features, while the second comprises four closely-separated strong

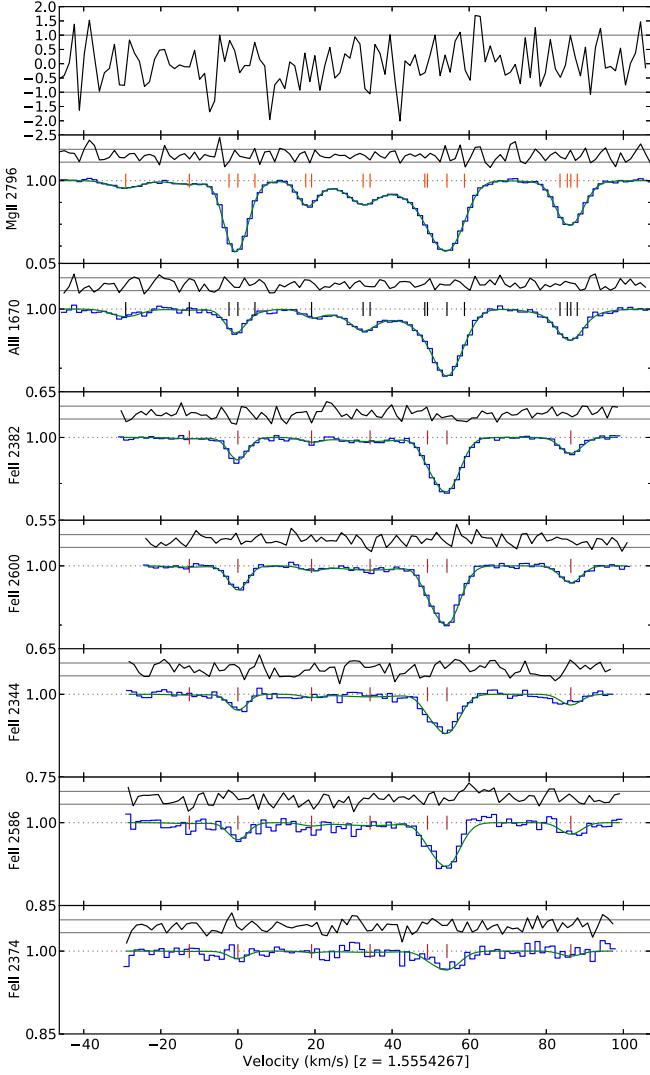


**Fig. 4.** Absorption profile for system at  $z_{\text{abs}} = 1.5558$  with transitions used in the second analysis approach for determining  $\Delta\alpha/\alpha$ . The figure is structured as in Fig. 2. Details of the absorption profile fit are given in Table 6.

features, but in both systems the strong features are broad and smooth with strong asymmetries. Thus, fairly complex absorption models were fitted to these systems, with the strong features comprising several velocity components of similar strength each.

The  $\chi^2$  minimization analysis of the profiles shown in Figs. 5 and 6, and the systematic error tests in Section 4.1.1, provide the following results:

$$\Delta\alpha/\alpha = \begin{cases} +21.4 \pm 24.2_{\text{stat}} \pm 20.9_{\text{sys}} \text{ ppm} & \text{at } z_{\text{abs}} = 0.9407, \\ +9.3 \pm 12.7_{\text{stat}} \pm 9.8_{\text{sys}} \text{ ppm} & \text{at } z_{\text{abs}} = 0.9424. \end{cases} \quad (7)$$

Given the relatively large statistical uncertainties on  $\Delta\alpha/\alpha$  in these absorbers, we neglect the systematic error budgets because they will be much smaller.

#### 4.5. Absorption system at $z_{\text{abs}} = 0.7866$

The transitions used to constrain  $\Delta\alpha/\alpha$  in the second analysis approach for the absorption system at  $z_{\text{abs}} = 0.7866$  are shown

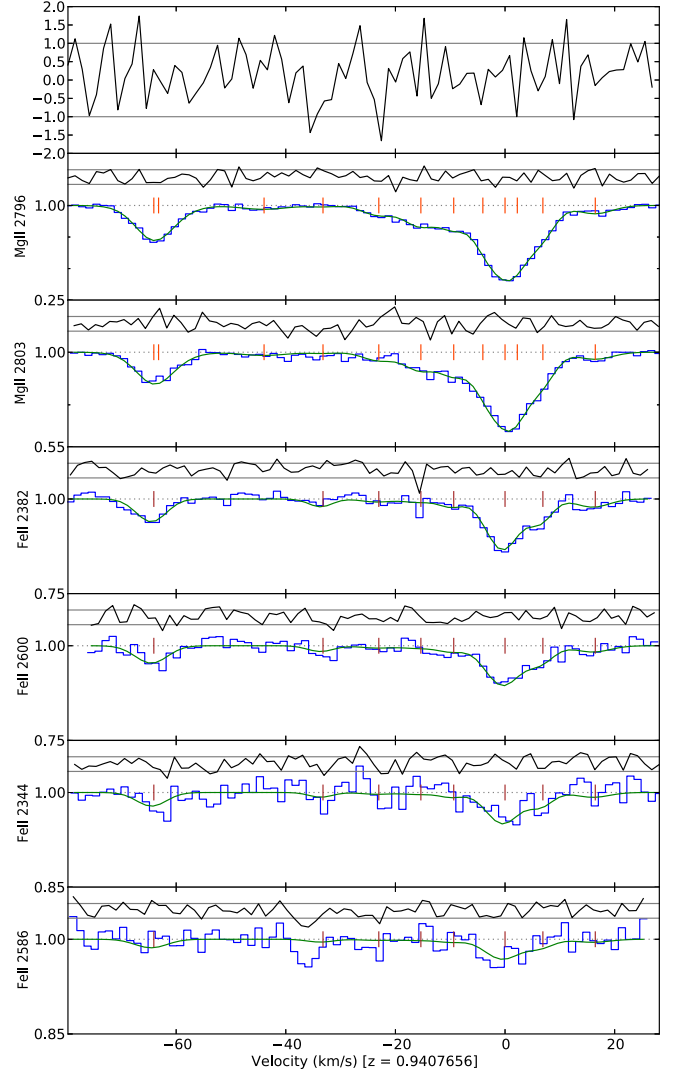


**Fig. 5.** Absorption profile for system at  $z_{\text{abs}} = 0.9407$  with transitions used in the second analysis approach for determining  $\Delta\alpha/\alpha$ . The figure is structured as in Fig. 2. Details of the absorption profile fit are given in Table 7.

in Fig. 7. The absorption profile model parameters from this approach are provided in Table 8. The absorption spans  $\sim 90 \text{ km s}^{-1}$  in one broad complex of several highly blended features, each of which shows visual evidence of asymmetries and none of which are particularly narrow. Thus, like all the other absorbers studied here, the main absorption features require several velocity components for an adequate fit. Detected transitions not used to constrain  $\Delta\alpha/\alpha$  include strong Si II  $\lambda 1526$  absorption which falls in the Ly $\alpha$  forest.

The  $\chi^2$  minimization analysis of the  $z_{\text{abs}} = 0.7866$  profiles shown in Fig. 7 and the systematic error tests in Section 4.1.1 provide a final result of

$$\Delta\alpha/\alpha = +7.3 \pm 35.9_{\text{stat}} \pm 21.4_{\text{sys}} \text{ ppm}. \quad (8)$$

Given the relatively large statistical uncertainty on  $\Delta\alpha/\alpha$  in this absorber, we neglect here the systematic error budget because it will be much smaller.

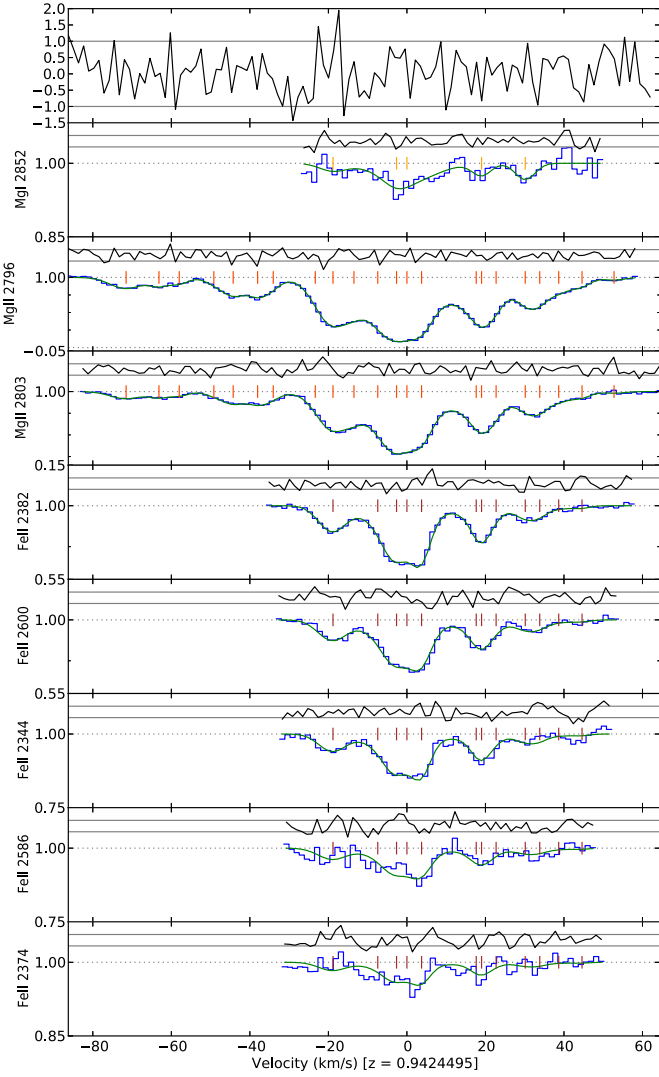


**Fig. 6.** Absorption profile for system at  $z_{\text{abs}} = 0.9424$  with transitions used in the second analysis approach for determining  $\Delta\alpha/\alpha$ . The figure is structured as in Fig. 2. Details of the absorption profile fit are given in Table 7.

## 5. Discussion

Present searches for cosmological variations in the fine-structure constant are based on the analysis of large samples of absorption systems observed at different redshifts and directions in the sky. Thanks to the large size of these samples it is possible to reach an ensemble sensitivity of a few ppm in  $\Delta\alpha/\alpha$ . On the other hand, deep observations of few selected lines of sight are capable of producing measurements with similar statistical errors. The two approaches have both intrinsic merits: the former is more effective in detecting possible changes as a function of redshift or across different regions of space, and possibly for averaging down systematic effects; the latter allows more detailed analysis, potentially facilitating the identification of possible systematic errors which may go undetected in a large number of systems.

The line of sight towards the relatively bright quasar HE 2217–2818 is rich with absorption systems. Our Many Multiplet analysis of the 5 systems observed at  $z_{\text{abs}} = 0.7866$ , 0.9407, 0.9424, 1.5558, 1.6279 and 1.6919 provides no evidence of a change of the fine-structure constant. In particular,

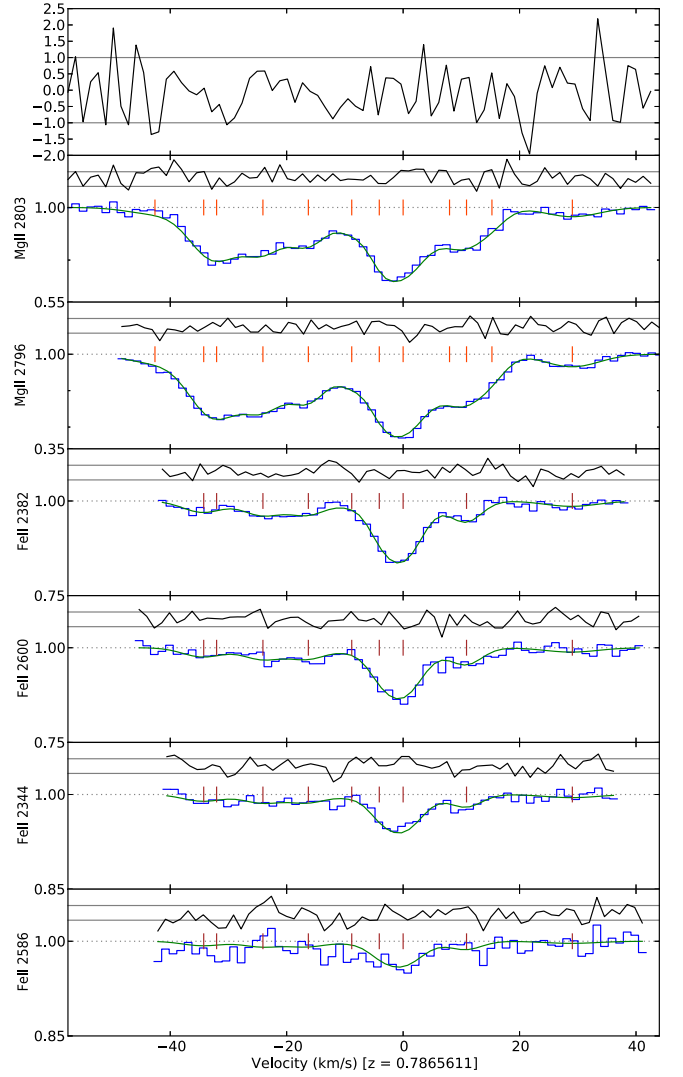


**Fig. 7.** Absorption profile for system at  $z_{\text{abs}} = 0.7866$  with transitions used in the second analysis approach for determining  $\Delta\alpha/\alpha$ . The figure is structured as in Fig. 2. Details of the absorption profile fit are given in Table 8.

the system at  $z_{\text{abs}} = 1.6919$  provides a very precise bound on variations in  $\alpha$ :  $\Delta\alpha/\alpha = +1.3 \pm 2.4_{\text{stat}} \pm 1.0_{\text{sys}}$  ppm. This result, stemming from our second analysis approach in which we conducted several tests to constrain the systematic error budget, differs somewhat from the first approach, conducted separately with different details of the data reduction, calibration and analysis:  $\Delta\alpha/\alpha = -3.8 \pm 2.1_{\text{stat}}$  ppm. This may indicate that systematic errors are larger than expected from the range of tests we conducted. However, it is interesting to note that restricting the first approach to the 6 Fe II transitions, and using a modified absorption model, yields a similar result to the second approach,  $\Delta\alpha/\alpha = +1.1 \pm 2.6_{\text{stat}}$  ppm. Clearly, it is important to continue to refine the analysis techniques to minimize differences in the results obtained by different approaches. Our future papers on this and other quasars in our Large Program of new VLT/UVES observations will aim at that goal.

The main reasons for the small statistical uncertainty in  $\Delta\alpha/\alpha$  from the  $z_{\text{abs}} = 1.6919$  absorber are the several narrow absorption features across its absorption profile, the inclusion of the Fe II  $\lambda 1608$  transition which, compared to the other Fe II

**Table 9.** Summary of  $\Delta\alpha/\alpha$  results including 1- $\sigma$  statistical uncertainties and estimated systematic errors for the 5 absorption systems towards HE 2217–2818 studied here. Our two separate analysis results for the absorber at  $z_{\text{abs}}=1.6919$  are identified in parentheses.

| $z$        | $\Delta\alpha/\alpha$<br>[ppm] | $\sigma_{\text{stat}}$<br>[ppm] | $\sigma_{\text{sys}}$<br>[ppm] | $\chi^2_{\nu}$ | Ions                       |
|------------|--------------------------------|---------------------------------|--------------------------------|----------------|----------------------------|
| 0.7866     | +7.32                          | 35.89                           | 21.36                          | 1.29           | Fe II, Mg II               |
| 0.9407     | +21.40                         | 24.16                           | 20.86                          | 1.13           | Fe II, Mg II               |
| 0.9424     | +9.32                          | 12.68                           | 9.84                           | 1.30           | Fe II, Mg II               |
| 1.5558     | -0.15                          | 24.90                           | 3.55                           | 1.21           | Fe II, Al II, Si II, Mg II |
| 1.6279     | +37.22                         | 20.62                           | 39.44                          | 1.43           | Fe II, Al II, Si II, Mg II |
| 1.6919 (A) | -3.84                          | 2.10                            |                                | 0.96           | Fe II, Al II               |
| 1.6919 (A) | +1.14                          | 2.58                            |                                | 0.94           | Fe II                      |
| 1.6919 (B) | +1.29                          | 2.35                            | 0.96                           | 1.19           | Fe II, Al II, III          |

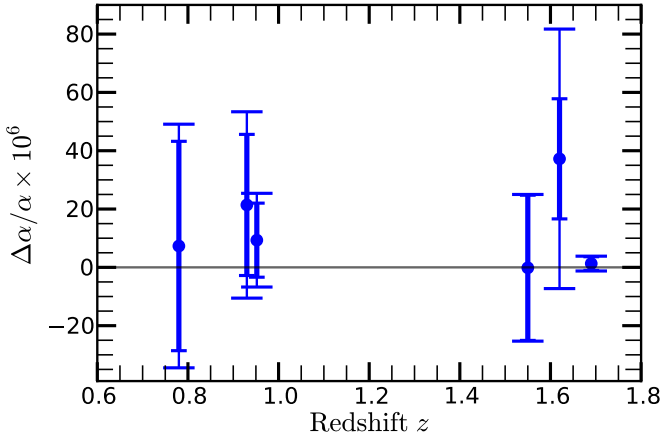


**Fig. 8.** Summary of  $\Delta\alpha/\alpha$  measurements towards HE 2217–2818. Each absorption system's  $\Delta\alpha/\alpha$  value from the second analysis approach is plotted with its 1- $\sigma$  statistical uncertainty, plus the total uncertainty formed by quadrature addition of the statistical and systematic errors in Table 9.

transitions in particular, provide a large range of  $q$ -coefficients among the fitted transitions, and the high S/N of the spectra. Unfortunately, the absorption features characterising the other 4 absorbers tended to be somewhat broader. And with a smaller range of  $q$  coefficients available from the fitted transitions, the statistical uncertainties in those absorbers exceeded 10 ppm.

The bound on  $\Delta\alpha/\alpha$  obtained from the  $z_{\text{abs}} = 1.6919$  system is one of the most precise measurements available from an individual absorber. Three other studies of individual absorbers have claimed measurements with comparably small uncertainties. These are  $\Delta\alpha/\alpha = -0.07 \pm 1.8$  ppm obtained from absorption at  $z_{\text{abs}} = 1.15$  towards the extremely bright quasar HE 0515–4414 (Molaro et al. 2008b),  $\Delta\alpha/\alpha = 5.4 \pm 2.5$  ppm from the system at  $z_{\text{abs}} = 1.84$  towards quasar Q 1101–264 (Levshakov et al. 2006), and  $\Delta\alpha/\alpha = -1.5 \pm 2.6$  ppm from the system at  $z_{\text{abs}} = 1.58$  towards HE 0001–2340 (Agafonova et al. 2011). The former two were both obtained by comparing only Fe II lines with each other, while the latter was derived through a comparison of Fe II and Si II transitions. The result at  $z_{\text{abs}} = 1.6919$  presented here was obtained by comparing Al II  $\lambda 1670$  and several Fe II transitions, including Fe II  $\lambda 1608$ . Broad agreement is found when using only the Fe II lines, particularly when considering the total systematic error budget of 2.4 ppm and the strong dependence on Fe II  $\lambda 1608$  in that case. Therefore,

we find no strong evidence for influence from differential ionization effects which may be present when comparing different ions.

Recently, King et al. (2012) analyzed a new sample of 153 measurements obtained from observations taken with UVES at the ESO Very Large Telescope (VLT), adding to the previous sample of 143 absorption systems obtained from the analysis of Keck/HIRES spectra (Murphy et al. 2003). The two samples generally probe different directions in the universe, and rather surprisingly they show different dependence on redshift; that is,  $\alpha$  appears on average to be smaller in the past in the northern hemisphere but larger in the past in the southern hemisphere. This is particularly the case for the combined dataset at redshift  $\geq 1.8$ . Overall, the variation across the sky can be simply and consistently represented by a monopole (i.e. a constant offset in  $\alpha$  from the current laboratory value) plus a spatial dipole in the direction with right ascension  $17.3 \pm 1.0$  hours and declination  $-61 \pm 10$  degrees (King et al. 2012). The spatial dependence is fitted with  $\Delta\alpha/\alpha = m + A \cos \Theta$ , where  $A$  is the dipole amplitude  $A = 9.7 \pm 2.1$  ppm,  $\Theta$  is the angle on the sky between a quasar sight-line and the best-fit dipole position, and  $m = -1.78 \pm 0.84$  ppm is the monopole term. A simpler model, without the monopole term, gives  $A = 10.2 \pm 2.1$  ppm with a pole towards right ascension  $17.4 \pm 0.9$  hours and declination  $-58 \pm 9$  degrees (King et al. 2012).

The dipole amplitude of  $\approx 10$  ppm could in principle be revealed by precise measurements along individual lines of sight. The pole and anti-pole directions are observationally difficult regions to study, particularly the pole which is very close to the Galactic center and virtually devoid of bright quasars. Towards the directions for which precise individual absorbers have been studied, the variation in  $\alpha$  expected by the dipole model is small and cannot be revealed by present accuracies<sup>6</sup>. However, the line of sight towards HE 2217–2818 subtends an angle  $\Theta = 58.8^\circ$  with respect to the simple dipole-only model above which is small enough to produce a signal which may be detectable along this single line of sight: the predicted signal is  $\Delta\alpha/\alpha = +5.4 \pm 1.7$  ppm. For a simple comparison with our main result here ( $\Delta\alpha/\alpha = +1.3 \pm 2.4_{\text{stat}} \pm 1.0_{\text{sys}}$  ppm), we combined its statistical and systematic error terms in quadrature, which reveals that it differs from this simple dipole prediction (including its uncertainty) by 1.3  $\sigma$ . The prediction from the monopole+dipole model at the sky position of HE 2217–2818 is  $\Delta\alpha/\alpha = +3.2 \pm 1.7$  ppm<sup>7</sup>. Thus, our most precise result towards HE 2217–2818 does not directly support evidence for a dipolar variation in  $\alpha$  across the sky, though it does not provide compelling evidence against it either.

## 6. Conclusions

The line of sight towards the relatively bright quasar HE 2217–2818 is rich with absorption systems and is located in the sky at a favourable position to probe the recently proposed presence of spatial variation of the fine structure constant,  $\alpha$ . It is the first quasar from our ongoing VLT/UVES Large Program to measure  $\Delta\alpha/\alpha$  in  $\sim 25$  absorbers towards  $\sim 12$  bright quasars

<sup>6</sup> The simple dipole model used here predicts the following values of  $\Delta\alpha/\alpha$  for the three quasars with previous precise measurements:  $2.6 \pm 1.4$  ppm (HE 0001–2340),  $2.2 \pm 1.6$  ppm (HE 0515–4414) and  $3.5 \pm 1.4$  ppm (Q 1101–264).

<sup>7</sup> A simple PYTHON program by J.B.W. for estimating the predicted dipole can be found at [http://pypi.python.org/pypi/dipole\\_error/](http://pypi.python.org/pypi/dipole_error/).

from which we expect to make  $\sim 20$  measurements of  $\Delta\alpha/\alpha$  with precision  $\lesssim 10$  ppm. Approximately 10 of these – the absorbers which are the main targets of the Large Program – will provide very high statistical precisions of  $\sim 2$  ppm each and systematic uncertainties  $\lesssim 2$  ppm. This will yield a final ensemble precision of better than 1 ppm with the additional aim of better understanding possible systematic uncertainties at this accuracy level. Our Many Multiplet analysis here of the 5 absorption systems observed at  $z_{\text{abs}} = 0.7866, 0.9407, 0.9424, 1.5558, 1.6279$  and  $1.6919$  is in-keeping with these goals: the highest-redshift absorber provides a very precise and robust measurement at the  $\sim 2$  ppm level while the 4 others provide weaker constraints  $\gtrsim 10$  ppm.

The high S/N, sharp absorption features and diversity of sensitivity to  $\alpha$  in the transitions of the  $z_{\text{abs}} = 1.6919$  absorber provides the most stringent measurement on  $\Delta\alpha/\alpha$  for this line of sight. Two separate approaches to the data-reduction, calibration and absorption line fitting yielded slightly different results –  $\Delta\alpha/\alpha = -3.8 \pm 2.1_{\text{stat}}$  ppm and  $\Delta\alpha/\alpha = +1.3 \pm 2.4_{\text{stat}}$  – though both are both consistent with no variation in  $\alpha$ . We also investigated a number of sources of systematic errors in this system and the effect that they might have on the final measurement. Our final result for this absorber, including both statistical and systematic error terms, is  $\Delta\alpha/\alpha = +1.3 \pm 2.4_{\text{stat}} \pm 1.0_{\text{sys}}$ . The results for the all absorption systems are summarized in Table 9.

If the evidence for a spatial variation of  $\alpha$  across the sky presented by Webb et al. (2011) and King et al. (2012) represents reality, then the simplest model of those results – a dipolar variation in  $\alpha$  – predicts  $\Delta\alpha/\alpha = 5.4 \pm 1.7$  ppm in the direction of the line of sight of HE 2217–2818. Our constraint on  $\Delta\alpha/\alpha$  from the  $z_{\text{abs}} = 1.6919$  absorber does not strongly support or conflict with that prediction.

*Acknowledgements.* An anonymous referee is acknowledged for several advices. P.M. and C.J.M. acknowledge support from grants PTDC/FIS/111725/2009 and PTDC/CTE-AST/098604/2008 from FCT, Portugal. The work of P.M. was partially funded by grant CAUP-06/2010-BCC. The work of C.J.M. is funded by a Ciência 2007 Research Contract, funded by FCT/MCTES (Portugal) and POPH/FSE (EC). M.T.M. thanks the Australian Research Council for funding under the *Discovery Projects* scheme (DP110100866). PPJ is supported in part by Agence Nationale pour la Recherche under contract ANR-10-Blan-0510-01. RS and PPJ gratefully acknowledge support from the Indo-French Centre for the Promotion of Advanced Research (Centre Franco-Indien pour la promotion de la recherche avance) under Project N.4304-2. SL has been supported by FONDECYT grant number 1100214. The work of I.I.A. and S.A.L. is supported by DFG Sonderforschungsbereich SFB 676 Teilprojekt C4 and, in part, by the State Program Leading Scientific Schools of Russian Federation (grant NSH 4035.2012.2)

## References

Agafonova, I.I., Molaro, P., Levshakov, S.A., & Hou, J.L. 2011, *A&A*, 529, 28  
 Amendola, L., Leite, A.C.O., Martins, C.J.A.P. et al 2012 *Phys. Rev D* 86, 063515  
 Bahcall, J.N., Sargent, W. L.W., & Schmidt, M. 1967, *ApJ*, 149, L11  
 Chand, H., Srianand, R., Petitjean, P., & Aracil, B. 2004, *A&A*, 417, 853  
 Dzuba, V.A., Flambaum, V.V., & Webb, J.K. 1999, *Phys. Rev. Lett.*, 82, 888  
 Edlén, B. 1966, *Metrologia*, 2, 71  
 Evans, T.M. & Murphy, M.T. 2013, *ApJ*, submitted  
 Griest, K., Whitmore, J.B., Wolfe, A.M., et al. 2010, *ApJ*, 708, 158  
 King J. A., Mortlock D. J., Webb J. K., Murphy M. T., 2009, *MmSAI*, 80, 864  
 King, J.A., Webb, J.K., Murphy, M.T., et al. 2012, *MNRAS*, 422, 3370  
 Levshakov, S.A., Centurión, M., Molaro, P., & D’Odorico, S. 2005, *A&A*, 434, 827

Levshakov, S.A., Centurión, M., Molaro, P., & Kostina, M.V. 2006, *A&A*, 447, L21  
 Lovis, C. & Pepe, F. 2007, *A&A*, 468, 1115  
 Molaro, P., Centurión, M., Monai, S., & Levshakov, S. 2011, *Spectrographs, Asteroids and Constants*, ed. C.Martins & P.Molaro, *Astrophysics and Space Science Proceedings* (Berlin Heidelberg: Springer-Verlag), 167  
 Molaro, P., Levshakov, S.A., Monai, S., et al. 2008a, *A&A*, 481, 559  
 Molaro, P., Reimers, D., Agafonova, I.I., & Levshakov, S.A. 2008b, *European Physical Journal Special Topics*, 163, 173  
 Murphy M. T., 2002, Probing variations in the fundamental constants with quasar absorption lines. PhD thesis, University of New South Wales  
 Murphy, M.T., Webb, J.K., & Flambaum, V.V. 2003, *MNRAS*, 345, 609  
 Murphy, M.T., Udem, T., Holzwarth, R., et al. 2007a, *MNRAS*, 380, 839  
 Murphy, M.T., Webb, J.K., & Flambaum, V.V. 2007b, *Phys. Rev. Lett.*, 99, 239001  
 Murphy, M.T., Webb, J.K., & Flambaum, V.V. 2008, *MNRAS*, 384, 1053  
 Murphy, M.T., Webb, J.K., Flambaum, V.V., et al. 2001, *MNRAS*, 327, 1208  
 Nave, G. & Sansonetti, C.J. 2011, *J. Opt. Soc. America B*, 28, 737  
 Olive, K.A., Peloso, M., & Uzan, J.-P. 2011, *Phys. Rev. D*, 83, 043509  
 Press, W. H., Teukolsky, S. A., Vetterling, W.T., Flannery, B. P. 1992, *Cambridge University Press* 1992  
 Quast, R., Reimers, D., & Levshakov, S.A. 2004, *A&A*, 415, L7  
 Savedoff, M.P. 1956, *Nat*, 178, 688  
 Srianand, R., Chand, H., Petitjean, P., Aracil, B. 2007, *PhRvL* 99, 9002  
 Webb, J.K., Flambaum, V.V., Churchill, C.W., Drinkwater, M.J., & Barrow, J.D. 1999, *Phys. Rev. Lett.*, 82, 884  
 Webb, J.K., King, J.A., Murphy, M.T., et al. 2011, *Phys. Rev. Lett.*, 107, 191101  
 Wendt, M. & Molaro, P. 2012, *A&A*, 541, 69  
 Whitmore, J.B., Murphy, M.T., & Griest, K. 2010, *ApJ*, 723, 89  
 Wilken, T., Lovis, C., Manescau, A., et al. 2010, *MNRAS*, 405, L16

**Table 4.** Multi-component Voigt profile model and  $\chi^2$  minimization results for the absorber at  $z_{\text{abs}} = 1.6919$ . The redshift ( $z$ ), Doppler broadening parameter ( $b$ ) and relevant column densities for each velocity component are presented, along with their 1- $\sigma$  uncertainties from `vFIT` are provided in the main section of the table. The fitted value for  $\Delta\alpha/\alpha$ , its 1- $\sigma$  statistical uncertainty (see text for systematic error component) and the final  $\chi^2$  per degree of freedom,  $\chi^2_{\nu}$ , are provided in the lower part.

| $z$                   | $\sigma_z$             | $b$                    | $\sigma_b$             | $\log N(\text{Fe II})$ | $\sigma_N$           | $\log N(\text{Al II})$ | $\sigma_N$           | $\log N(\text{Al III})$ | $\sigma_N$           |
|-----------------------|------------------------|------------------------|------------------------|------------------------|----------------------|------------------------|----------------------|-------------------------|----------------------|
|                       |                        | [ $\text{km s}^{-1}$ ] | [ $\text{km s}^{-1}$ ] | [ $\text{cm}^{-2}$ ]   | [ $\text{cm}^{-2}$ ] | [ $\text{cm}^{-2}$ ]   | [ $\text{cm}^{-2}$ ] | [ $\text{cm}^{-2}$ ]    | [ $\text{cm}^{-2}$ ] |
| 1.6904350             | 0.0000070              | 3.7                    | 1.4                    | 10.99                  | 0.18                 |                        |                      |                         |                      |
| 1.6905417             | 0.0000087              | 9.0                    | 1.4                    | 11.50                  | 0.07                 | 11.24                  | 0.06                 | 11.19                   | 0.10                 |
| 1.6907366             | 0.0000068              | 3.1                    | 1.4                    | 10.92                  | 0.16                 | 10.72                  | 0.11                 | 10.77                   | 0.20                 |
| 1.6908227             | 0.0000019              | 3.8                    | 0.6                    | 11.87                  | 0.08                 | 11.33                  | 0.12                 | 11.33                   | 0.09                 |
| 1.6909516             | 0.0000071              | 11.7                   | 1.9                    | 12.27                  | 0.04                 | 11.93                  | 0.04                 | 11.56                   | 0.13                 |
| 1.6909735             | 0.0000005              | 2.6                    | 0.1                    | 12.67                  | 0.01                 | 11.78                  | 0.03                 | 11.21                   | 0.11                 |
| 1.6910942             | 0.0000022              | 1.2                    | 1.1                    | 11.46                  | 0.07                 | 10.93                  | 0.09                 |                         |                      |
| 1.6911884             | 0.0000037              | 4.1                    | 0.6                    | 12.34                  | 0.44                 | 11.92                  | 0.28                 | 11.62                   | 0.22                 |
| 1.6912232             | 0.0000218              | 5.6                    | 1.3                    | 12.51                  | 0.31                 | 11.84                  | 0.35                 | 11.38                   | 0.39                 |
| 1.6912519             | 0.0000317              | 25.5                   | 6.5                    | 10.90                  | 0.99                 | 11.45                  | 0.14                 | 11.82                   | 0.08                 |
| 1.6913146             | 0.0000079              | 6.0                    | 0.9                    | 11.87                  | 0.11                 | 11.46                  | 0.10                 |                         |                      |
| 1.6915804             | 0.0000036              | 5.3                    | 0.8                    | 11.45                  | 0.05                 | 11.17                  | 0.05                 | 11.04                   | 0.15                 |
| 1.6916675             | 0.0000059              | 1.7                    | 1.8                    | 10.75                  | 0.18                 | 10.60                  | 0.13                 |                         |                      |
| 1.6919120             | 0.0000159              | 13.8                   | 1.8                    | 11.18                  | 0.15                 | 11.65                  | 0.07                 | 11.85                   | 0.07                 |
| 1.6920159             | 0.0000080              | 5.2                    | 1.0                    | 11.71                  | 0.11                 | 11.45                  | 0.15                 | 11.24                   | 0.22                 |
| 1.6921268             | 0.0000167              | 6.0                    | 1.8                    | 12.27                  | 0.20                 | 12.08                  | 0.20                 | 11.63                   | 0.23                 |
| 1.6921421             | 0.0000025              | 0.5                    | 0.3                    | 11.83                  | 0.14                 | 11.24                  | 0.39                 | 10.50                   | 0.68                 |
| 1.6921871             | 0.0000155              | 2.4                    | 3.4                    | 11.27                  | 1.24                 | 11.11                  | 1.10                 | 11.05                   | 0.55                 |
| 1.6922586             | 0.0000231              | 10.4                   | 3.4                    | 11.59                  | 0.19                 | 11.67                  | 0.16                 | 11.64                   | 0.16                 |
| 1.6924106             | 0.0000037              | 3.7                    | 0.8                    | 11.57                  | 0.07                 | 11.33                  | 0.09                 | 11.22                   | 0.10                 |
| 1.6924667             | 0.0000040              | 0.5                    | 2.0                    | 11.30                  | 0.17                 | 11.14                  | 0.58                 |                         |                      |
| 1.6925374             | 0.0000061              | 5.3                    | 1.1                    | 12.29                  | 0.09                 | 11.92                  | 0.09                 | 11.61                   | 0.09                 |
| 1.6926068             | 0.0000029              | 3.6                    | 0.5                    | 12.31                  | 0.08                 | 11.82                  | 0.11                 | 11.43                   | 0.14                 |
| 1.6926757             | 0.0000106              | 3.4                    | 2.5                    | 11.12                  | 0.52                 | 11.07                  | 0.36                 | 11.19                   | 0.22                 |
| 1.6927497             | 0.0000095              | 4.7                    | 1.1                    | 12.04                  | 0.30                 | 11.84                  | 0.25                 | 11.50                   | 0.32                 |
| 1.6928042             | 0.0000010              | 2.6                    | 0.3                    | 12.54                  | 0.10                 | 11.89                  | 0.18                 | 11.22                   | 0.46                 |
| 1.6928307             | 0.0000648              | 6.7                    | 4.8                    | 12.01                  | 0.65                 | 11.69                  | 0.62                 | 11.44                   | 0.60                 |
| 1.6929678             | 0.0000116              | 4.0                    | 3.3                    | 11.09                  | 0.37                 | 10.76                  | 0.53                 |                         |                      |
| 1.6930588             | 0.0000248              | 12.3                   | 2.4                    | 11.45                  | 0.22                 | 11.47                  | 0.13                 |                         |                      |
| 1.6930679             | 0.0000026              | 3.1                    | 0.9                    | 11.52                  | 0.10                 | 10.77                  | 0.22                 |                         |                      |
| 1.6933236             | 0.0000021              | 2.7                    | 0.5                    | 11.42                  | 0.03                 | 10.73                  | 0.06                 |                         |                      |
| 1.6934849             | 0.0000126              | 4.0                    | 2.5                    | 10.82                  | 0.15                 |                        |                      |                         |                      |
| $\Delta\alpha/\alpha$ | $\sigma_{\text{stat}}$ | $\chi^2_{\nu}$         |                        |                        |                      |                        |                      |                         |                      |
| [ppm]                 | [ppm]                  |                        |                        |                        |                      |                        |                      |                         |                      |
| +1.29                 | 2.35                   | 1.19                   |                        |                        |                      |                        |                      |                         |                      |

**Table 5.** As in Table 4 but for the absorption system at  $z_{\text{abs}} = 1.6279$ .

| $z$                   | $\sigma_z$             | $b$                   | $\sigma_b$            | $\log N(\text{Al II})$ | $\sigma_N$          | $\log N(\text{Al III})$ | $\sigma_N$          | $\log N(\text{Mg II})$ | $\sigma_N$          | $\log N(\text{Mg I})$ | $\sigma_N$          |
|-----------------------|------------------------|-----------------------|-----------------------|------------------------|---------------------|-------------------------|---------------------|------------------------|---------------------|-----------------------|---------------------|
|                       |                        | [km s <sup>-1</sup> ] | [km s <sup>-1</sup> ] | [cm <sup>-2</sup> ]    | [cm <sup>-2</sup> ] | [cm <sup>-2</sup> ]     | [cm <sup>-2</sup> ] | [cm <sup>-2</sup> ]    | [cm <sup>-2</sup> ] | [cm <sup>-2</sup> ]   | [cm <sup>-2</sup> ] |
| 1.6272489             | 0.0000071              | 5.7                   | 0.9                   | 10.69                  | 0.10                | 10.30                   | 0.47                | 11.48                  | 0.07                | 9.96                  | 0.20                |
| 1.6273505             | 0.0000094              | 4.9                   | 1.3                   | 11.13                  | 0.14                | 10.79                   | 0.26                | 11.81                  | 0.15                |                       |                     |
| 1.6274298             | 0.0000342              | 4.3                   | 3.1                   | 11.26                  | 0.71                | 11.36                   | 0.57                | 12.04                  | 0.71                | 10.28                 | 0.47                |
| 1.6274753             | 0.0000080              | 3.8                   | 1.5                   | 11.76                  | 0.27                | 11.61                   | 0.40                | 12.54                  | 0.27                | 10.19                 | 0.74                |
| 1.6275091             | 0.0000076              | 0.5                   | 1.0                   | 10.84                  | 0.55                | 11.14                   | 0.25                | 11.77                  | 0.36                | 10.02                 | 0.28                |
| 1.6275388             | 0.0000048              | 1.0                   | 0.7                   | 10.97                  | 0.34                | 11.01                   | 0.28                | 11.80                  | 0.25                | 9.88                  | 0.27                |
| 1.6275714             | 0.0000215              | 5.0                   | 3.1                   | 11.29                  | 0.30                | 11.21                   | 0.30                | 11.98                  | 0.30                |                       |                     |
| 1.6276866             | 0.0000333              | 4.0                   | 1.7                   | 11.74                  | 1.00                | 11.33                   | 1.30                | 12.54                  | 0.93                | 10.61                 | 0.64                |
| 1.6277150             | 0.0000071              | 2.9                   | 0.6                   | 11.45                  | 0.65                | 10.87                   | 2.08                | 12.37                  | 0.40                | 10.38                 | 0.75                |
| 1.6277377             | 0.0001969              | 4.9                   | 18.5                  | 11.34                  | 3.06                | 11.15                   | 3.07                | 12.05                  | 3.07                | 9.57                  | 3.04                |
| 1.6278005             | 0.0000141              | 4.3                   | 1.8                   | 11.29                  | 0.26                | 11.15                   | 0.26                | 12.15                  | 0.21                |                       |                     |
| 1.6278641             | 0.0000061              | 4.3                   | 1.0                   | 11.74                  | 0.12                | 11.45                   | 0.14                | 12.61                  | 0.13                | 10.74                 | 0.09                |
| 1.6279165             | 0.0000063              | 2.5                   | 1.2                   | 11.48                  | 0.46                | 11.28                   | 0.49                | 12.42                  | 0.39                | 10.22                 | 0.56                |
| 1.6279655             | 0.0000083              | 4.0                   | 2.3                   | 11.97                  | 0.25                | 11.85                   | 0.23                | 12.83                  | 0.25                | 10.74                 | 0.25                |
| 1.6280013             | 0.0000079              | 1.2                   | 2.0                   | 11.11                  | 0.74                | 10.54                   | 1.92                | 11.91                  | 0.85                | 9.96                  | 0.69                |
| 1.6280395             | 0.0000153              | 3.7                   | 2.4                   | 11.53                  | 0.29                | 11.49                   | 0.27                | 12.29                  | 0.31                | 10.13                 | 0.37                |
| 1.6280932             | 0.0000041              | 0.7                   | 0.5                   | 10.78                  | 0.22                | 10.36                   | 0.60                | 11.72                  | 0.14                | 9.33                  | 0.69                |
| 1.6281297             | 0.0000036              | 0.8                   | 0.6                   | 10.82                  | 0.06                | 10.80                   | 0.16                | 11.51                  | 0.07                | 9.42                  | 0.55                |
| 1.6281677             | 0.0000054              | 0.5                   | 1.7                   | 10.36                  | 0.17                | 10.61                   | 0.25                | 11.11                  | 0.14                | 9.73                  | 0.25                |
| 1.6282117             | 0.0000062              | 8.2                   | 0.6                   | 11.12                  | 0.06                | 10.93                   | 0.17                | 12.00                  | 0.04                |                       |                     |
| $\Delta\alpha/\alpha$ | $\sigma_{\text{stat}}$ | $\chi^2_{\nu}$        |                       |                        |                     |                         |                     |                        |                     |                       |                     |
| [ppm]                 | [ppm]                  |                       |                       |                        |                     |                         |                     |                        |                     |                       |                     |
| +37.22                | 20.62                  | 1.43                  |                       |                        |                     |                         |                     |                        |                     |                       |                     |

**Table 6.** As in Table 4 but for the absorption system at  $z_{\text{abs}} = 1.5558$ .

| $z$                   | $\sigma_z$             | $b$                   | $\sigma_b$            | $\log N(\text{Mg II})$ | $\sigma_N$          | $\log N(\text{Al II})$ | $\sigma_N$          | $\log N(\text{Fe II})$ | $\sigma_N$          |
|-----------------------|------------------------|-----------------------|-----------------------|------------------------|---------------------|------------------------|---------------------|------------------------|---------------------|
|                       |                        | [km s <sup>-1</sup> ] | [km s <sup>-1</sup> ] | [cm <sup>-2</sup> ]    | [cm <sup>-2</sup> ] | [cm <sup>-2</sup> ]    | [cm <sup>-2</sup> ] | [cm <sup>-2</sup> ]    | [cm <sup>-2</sup> ] |
| 1.5551786             | 0.0000039              | 4.4                   | 0.7                   | 11.28                  | 0.05                |                        |                     | 10.61                  | 0.18                |
| 1.5553193             | 0.0000162              | 5.2                   | 2.1                   | 11.01                  | 0.12                | 10.55                  | 0.66                | 9.83                   | 1.69                |
| 1.5554070             | 0.0000120              | 0.5                   | 1.0                   | 12.44                  | 1.93                |                        |                     | 10.46                  | 0.44                |
| 1.5554267             | 0.0000046              | 1.3                   | 0.4                   | 13.04                  | 0.78                | 11.63                  | 0.02                | 10.77                  | 0.31                |
| 1.5554644             | 0.0000496              | 2.8                   | 7.8                   | 10.86                  | 1.14                |                        |                     | 10.09                  | 1.26                |
| 1.5555767             | 0.0000074              | 0.5                   | 3.1                   | 11.63                  | 0.78                |                        |                     |                        |                     |
| 1.5555896             | 0.0000052              | 1.4                   | 1.8                   | 11.24                  | 0.59                | 10.85                  | 0.24                | 10.38                  | 0.30                |
| 1.5557036             | 0.0000026              | 2.1                   | 1.1                   | 11.37                  | 0.16                |                        |                     | 10.60                  | 0.22                |
| 1.5557190             | 0.0000094              | 10.7                  | 2.5                   | 11.89                  | 0.08                | 11.34                  | 0.08                | 11.12                  | 0.09                |
| 1.5558400             | 0.0000474              | 4.9                   | 3.3                   | 11.83                  | 0.65                |                        |                     | 10.99                  | 0.65                |
| 1.5558459             | 0.0000062              | 0.5                   | 1.0                   | 11.13                  | 0.72                | 11.36                  | 0.21                | 9.88                   | 2.07                |
| 1.5558890             | 0.0000050              | 3.4                   | 0.3                   | 12.47                  | 0.15                | 12.16                  | 0.03                | 11.47                  | 0.21                |
| 1.5559277             | 0.0000161              | 3.0                   | 1.4                   | 11.45                  | 0.38                |                        |                     | 10.81                  | 0.30                |
| 1.5561390             | 0.0000372              | 1.1                   | 4.6                   | 11.55                  | 1.35                |                        |                     | 10.27                  | 1.38                |
| 1.5561551             | 0.0000132              | 8.3                   | 2.6                   | 11.15                  | 0.49                |                        |                     | 10.93                  | 0.22                |
| 1.5561629             | 0.0000047              | 2.1                   | 0.4                   | 11.74                  | 8.58                | 11.49                  | 0.03                | 10.75                  | 5.19                |
| 1.5561771             | 0.0003294              | 2.4                   | 16.0                  | 11.58                  | 11.21               |                        |                     | 10.39                  | 10.88               |
| $\Delta\alpha/\alpha$ | $\sigma_{\text{stat}}$ | $\chi^2_{\nu}$        |                       |                        |                     |                        |                     |                        |                     |
| [ppm]                 | [ppm]                  |                       |                       |                        |                     |                        |                     |                        |                     |
| -0.15                 | 24.90                  | 1.21                  |                       |                        |                     |                        |                     |                        |                     |

**Table 7.** As in Table 4 but for the absorption systems at  $z_{\text{abs}} = 0.9407$  and  $z_{\text{abs}} = 0.9424$ .

| $z$                            | $\sigma_z$                      | $b$<br>[km s <sup>-1</sup> ] | $\sigma_b$<br>[km s <sup>-1</sup> ] | $\log N(\text{Mg II})$<br>[cm <sup>-2</sup> ] | $\sigma_N$<br>[cm <sup>-2</sup> ] | $\log N(\text{Fe II})$<br>[cm <sup>-2</sup> ] | $\sigma_N$<br>[cm <sup>-2</sup> ] | $\log N(\text{Mg I})$<br>[cm <sup>-2</sup> ] | $\sigma_N$<br>[cm <sup>-2</sup> ] |
|--------------------------------|---------------------------------|------------------------------|-------------------------------------|---|-----------------------------------|---|-----------------------------------|--|-----------------------------------|
| 0.9419861                      | 0.0000024                       | 4.5                          | 0.7                                 | 11.58   | 0.03                              |   |                                   |  |                                   |
| 0.9420403                      | 0.0000037                       | 0.5                          | 1.1                                 | 11.28   | 0.13                              |   |                                   |  |                                   |
| 0.9420738                      | 0.0000039                       | 0.5                          | 1.7                                 | 11.16   | 0.15                              |   |                                   |  |                                   |
| 0.9421309                      | 0.0000122                       | 0.5                          | 3.2                                 | 11.07   | 0.44                              |   |                                   |  |                                   |
| 0.9421628                      | 0.0000051                       | 2.0                          | 3.3                                 | 11.66   | 0.25                              |   |                                   |  |                                   |
| 0.9422031                      | 0.0000095                       | 1.7                          | 3.6                                 | 11.65   | 0.33                              |   |                                   |  |                                   |
| 0.9422289                      | 0.0000151                       | 0.5                          | 2.2                                 | 11.25   | 0.58                              |   |                                   |  |                                   |
| 0.9422983                      | 0.0000761                       | 4.9                          | 9.3                                 | 11.40   | 1.40                              |   |                                   |  |                                   |
| 0.9423275                      | 0.0000031                       | 3.8                          | 0.6                                 | 12.35   | 0.17                              | 11.86   | 0.07                              | 9.99   | 0.23                              |
| 0.9423621                      | 0.0000040                       | 0.5                          | 0.5                                 | 11.73   | 0.15                              |   |                                   |  |                                   |
| 0.9424014                      | 0.0000491                       | 5.1                          | 8.8                                 | 12.14   | 0.92                              | 11.53   | 0.92                              |  |                                   |
| 0.9424324                      | 0.0000039                       | 3.3                          | 1.0                                 | 12.44   | 0.45                              | 12.08   | 0.27                              | 9.96   | 0.65                              |
| 0.9424495                      | 0.0000130                       | 9.6                          | 2.8                                 | 12.48   | 0.28                              | 11.83   | 0.44                              | 10.70  | 0.13                              |
| 0.9424737                      | 0.0000027                       | 1.8                          | 0.6                                 | 12.28   | 0.14                              | 12.06   | 0.10                              |  |                                   |
| 0.9425639                      | 0.0000308                       | 6.7                          | 4.3                                 | 12.19   | 0.40                              | 11.53   | 0.47                              |  |                                   |
| 0.9425727                      | 0.0000032                       | 1.5                          | 1.0                                 | 12.04   | 0.27                              | 11.79   | 0.15                              | 10.04  | 0.17                              |
| 0.9425967                      | 0.0000107                       | 1.6                          | 3.6                                 | 11.62   | 0.80                              | 11.01   | 0.80                              |  |                                   |
| 0.9426448                      | 0.0000048                       | 1.9                          | 1.7                                 | 11.81   | 0.26                              | 11.36   | 0.21                              | 10.19  | 0.13                              |
| 0.9426687                      | 0.0000053                       | 0.5                          | 0.7                                 | 11.79   | 0.18                              | 11.18   | 0.23                              |  |                                   |
| 0.9427000                      | 0.0000077                       | 2.6                          | 3.8                                 | 11.60   | 0.30                              | 10.84   | 0.41                              |  |                                   |
| 0.9427385                      | 0.0000069                       | 0.5                          | 1.2                                 | 11.28   | 0.22                              | 10.62   | 0.27                              |  |                                   |
| 0.9427913                      | 0.0000064                       | 2.1                          | 2.9                                 | 10.77   | 0.14                              |   |                                   |  |                                   |
| $\Delta\alpha/\alpha$<br>[ppm] | $\sigma_{\text{stat}}$<br>[ppm] | $\chi^2_{\nu}$               |                                     |   |                                   |   |                                   |  |                                   |
| +9.32                          | 12.7                            | 1.30                         |                                     |   |                                   |   |                                   |  |                                   |
| 0.9403508                      | 0.0000033                       | 2.5                          | 0.8                                 | 11.48   | 0.33                              | 11.33   | 0.05                              |  |                                   |
| 0.9403564                      | 0.0000052                       | 5.0                          | 1.6                                 | 11.55   | 0.27                              |   |                                   |  |                                   |
| 0.9404810                      | 0.0000098                       | 4.9                          | 3.0                                 | 10.85   | 0.14                              |   |                                   |  |                                   |
| 0.9405506                      | 0.0000068                       | 0.5                          | 7.4                                 | 10.16   | 0.46                              | 10.76   | 0.20                              |  |                                   |
| 0.9406165                      | 0.0000102                       | 2.3                          | 2.7                                 | 11.11   | 0.23                              | 10.42   | 0.36                              |  |                                   |
| 0.9406662                      | 0.0000043                       | 2.4                          | 2.7                                 | 11.47   | 0.17                              | 10.49   | 0.39                              |  |                                   |
| 0.9407050                      | 0.0000057                       | 0.5                          | 0.6                                 | 11.50   | 0.11                              | 10.76   | 0.15                              |  |                                   |
| 0.9407394                      | 0.0000195                       | 1.0                          | 3.6                                 | 11.50   | 0.83                              |   |                                   |  |                                   |
| 0.9407656                      | 0.0000033                       | 3.0                          | 0.6                                 | 12.07   | 0.73                              | 11.73   | 0.03                              |  |                                   |
| 0.9407801                      | 0.0000229                       | 1.2                          | 5.0                                 | 11.65   | 1.35                              |   |                                   |  |                                   |
| 0.9408103                      | 0.0000033                       | 0.9                          | 0.8                                 | 11.63   | 0.07                              | 11.24   | 0.08                              |  |                                   |
| 0.9408722                      | 0.0000038                       | 3.0                          | 1.3                                 | 11.07   | 0.07                              | 10.91   | 0.12                              |  |                                   |
| $\Delta\alpha/\alpha$<br>[ppm] | $\sigma_{\text{stat}}$<br>[ppm] | $\chi^2_{\nu}$               |                                     |   |                                   |   |                                   |  |                                   |
| +21.40                         | 24.2                            | 1.13                         |                                     |   |                                   |   |                                   |  |                                   |

**Table 8.** As in Table 4 but for the absorption system at  $z_{\text{abs}} = 0.7866$ .

| $z$                            | $\sigma_z$                      | $b$<br>[km s <sup>-1</sup> ] | $\sigma_b$<br>[km s <sup>-1</sup> ] | $\log N(\text{Mg II})$<br>[cm <sup>-2</sup> ] | $\sigma_N$<br>[cm <sup>-2</sup> ] | $\log N(\text{Fe II})$<br>[cm <sup>-2</sup> ] | $\sigma_N$<br>[cm <sup>-2</sup> ] |
|--------------------------------|---------------------------------|------------------------------|-------------------------------------|---|-----------------------------------|---|-----------------------------------|
| 0.7863071                      | 0.0000787                       | 5.8                          | 10.8                                | 11.20   | 1.23                              |   |                                   |
| 0.7863570                      | 0.0000483                       | 3.7                          | 5.5                                 | 11.21   | 10.38                             | 11.11   | 2.40                              |
| 0.7863702                      | 0.0000753                       | 4.6                          | 2.7                                 | 12.04   | 1.53                              | 8.98  | 380.73                            |
| 0.7864176                      | 0.0000086                       | 3.4                          | 4.3                                 | 11.90   | 0.58                              | 11.19   | 0.55                              |
| 0.7864641                      | 0.0000091                       | 3.5                          | 2.9                                 | 11.87   | 0.30                              | 11.18   | 0.30                              |
| 0.7865085                      | 0.0000065                       | 1.2                          | 2.2                                 | 11.44   | 0.17                              | 10.52   | 0.47                              |
| 0.7865367                      | 0.0000047                       | 0.5                          | 0.8                                 | 11.75   | 0.24                              | 11.09   | 0.61                              |
| 0.7865611                      | 0.0000067                       | 3.7                          | 1.2                                 | 12.14   | 0.18                              | 11.85   | 0.12                              |
| 0.7866086                      | 0.0001375                       | 5.0                          | 22.5                                | 11.81   | 2.81                              |   |                                   |
| 0.7866260                      | 0.0000052                       | 2.3                          | 1.0                                 | 11.46   | 3.37                              | 11.29   | 0.06                              |
| 0.7866520                      | 0.0000245                       | 1.8                          | 8.5                                 | 11.31   | 3.32                              |   |                                   |
| 0.7867343                      | 0.0000040                       | 5.6                          | 1.1                                 | 11.36   | 0.05                              | 10.90   | 0.11                              |
| $\Delta\alpha/\alpha$<br>[ppm] | $\sigma_{\text{stat}}$<br>[ppm] | $\chi^2_{\nu}$               |                                     |   |                                   |   |                                   |
| +7.32                          | 35.89                           | 1.29                         |                                     |   |                                   |   |                                   |